CONF-8906324--1-Rev.

DE91 004441

REVISED OCTOBER 1990

RIETVELD REFINEMENT WITH TIME-OF-FLIGHT POWDER DIFFRACTION DATA FROM PULSED NEUTRON SOURCES

W. I. F. David
Neutron Science Division
Rutherford Appleton Laboratory
Chilton, Didcot, Oxon 0X11 OQX, UK

and

J. D. Jorgensen
Materials Science Division and
Argonne National Laboratory
Argonne, IL 60439 USA

DEC 0 4 1990

The submitted manuscript has been authored by a contractor of the U.S. Government under contract No. W-31-109-ENG-38. Accordingly, the U.S. Government retains a nonexclusive, royalty-free license to publish or reproduce the published form of this contribution, or allow others to do so, for U.S. Government purposes.

October, 1990

/sm

DISCLAIMER

This report was prepared as an account of work sponsored by an agency of the United States Government. Neither the United States Government nor any agency thereof, nor any of their employees, makes any warranty, express or implied, or assumes any legal liability or responsibility for the accuracy, completeness, or usefulness of any information, apparatus, product, or process disclosed, or represents that its use would not infringe privately owned rights. Reference herein to any specific commercial product, process, or service by trade name, trademark, manufacturer, or otherwise does not necessarily constitute or imply its endorsement, recommendation, or favoring by the United States Government or any agency thereof. The views and opinions of authors expressed herein do not necessarily state or reflect those of the United States Government or any agency thereof.

Invited Manuscript submitted to the Proceedings of the International Workshop on the Rietveld Method, Petten, Netherlands, 13-15 June 1989

This work is supported by the U.S. Department of Energy, Basic Energy Sciences, Materials Sciences, under contract No. W-31-109-ENG-38.

MASTER

DISTRIBUTION OF THIS DOCUMENT IS UNLIMITED

Rietveld Refinement with Time-of-Flight Powder Diffraction Data from Pulsed Neutron Sources

W. I. F. David
Neutron Science Division
Rutherford Appleton Laboratory
Chilton, Didcot, Oxon 0X11 OQX, UK

and

J. D. Jorgensen
Materials Science Division
Argonne National Laboratory,
Argonne, IL 60439 USA

Revised: 3 October 1990

Invited Manuscript submitted to the Proceedings of the International Workshop on the Rietveld Method, Petten, Netherlands, 13-15 June 1989

Rietveld Refinement with Time-of-Flight Powder Diffraction Data from Pulsed Neutron Sources

W. I. F. David Neutron Science Division, Rutherford Appleton Laboratory, Chilton, Didcot, Oxon 0X11 OQX, UK

and

J. D. Jorgensen, Materials Science Division, Argonne National Laboratory, Argonne, IL 60439 USA

INTRODUCTION

The recent development of accelerator-based pulsed neutron sources has led to the widespread use of the time-of-flight technique for neutron powder diffraction. The properties of the pulsed source make possible unusually high resolution over a wide range of d spacings, high count rates, and the ability to collect complete data at fixed scattering angles. The peak shape and other instrument characteristics can be accurately modelled, which makes Rietveld refinement possible for complex structures. In this paper we briefly review the development of the Rietveld method for time-of-flight diffraction data from pulsed neutron sources and discuss the latest developments in high resolution instrumentation and advanced Rietveld analysis methods.

EARLY HISTORY OF THE TIME-OF-FLIGHT RIETVELD METHOD

The first Rietveld refinement using time-of-flight neutron powder diffraction data was performed in 1974 to analyze the monoclinic phase of KCN from data taken in a high pressure cell [Decker et al 1974]. This experiment was part of an extended program using the time-of-flight technique with a neutron chopper on a reactor source to study the structures of materials at high pressure. The time-of-flight technique was chosen for this work because it made possible the collection of data at a fixed scattering angle for which the scattering from the pressure cell could be excluded by viewing the scattered neutrons only through a narrow window in the cell.

The time-of-flight technique proved ideal for structural studies at high pressure and a number of experiments [Worlton & Beyerlein 1975, Jorgensen et al 1978, Jorgensen 1978, Cartz et al 1979, Jorgensen & Clark 1980, Cartz & Jorgensen 1981, Jorgensen et al 1984] were performed between 1974 and 1979 using two different time-of-flight

The submitted manuscript has been authored by a contractor of the U. S. Government under contract No. W-31-109-ENG-38. Accordingly, the U. S. Government retains a nonexclusive, royalty-free license to publish or reproduce the published form of this

diffractometers at Argonne's CP-5 reactor. In all of these cases the data were analyzed by the Rietveld method.

The first analysis code for time-of-flight data was written at Argonne National Laboratory and incorporated features that specifically addressed the problems encountered in high pressure diffraction experiments [Worlton et al 1976]. For example, the code was capable of fitting up to four phases. This feature was included so that data from a pressure calibrant such as CsCl could be analyzed along with the sample data. The sample pressure was then accurately determined from the refined lattice constant for the calibrant. These first codes for Rietveld analysis of time-of-flight data were not actually based on the constant-wavelength code developed by Rietveld [1969] (and were, in fact, written with no knowledge of Rietveld's earlier work). There were three important differences. First, and most obvious, the extrinsic variable was time-of-flight, not scattering angle. Second, the variation of the resolution function with time-of-flight could be described by a simple function,

$$R(d) = \Delta d/d = (A + Bd^2)^{1/2}, \qquad (1)$$

where d is the d spacing, which is linearly proportional to the time-of-flight, t, and A and B are instrumental constants. Third, since the flux on the sample is a function of wavelength, the calculated intensity model included a wavelength-dependent term for the incident flux.

TIME-OF-FLIGHT DIFFRACTOMETERS AT REACTOR SOURCES

Although the resolution of the early reactor-based time-of-flight diffractometers was not high by present standards ($\Delta d/d \geq 0.006$) [Worlton et al 1976], the peak shape function was almost perfectly Gaussian as is shown in Figure 1. This ability to model accurately the peak shape and its wavelength dependence undoubtedly led to the success of the Rietveld method for this application. However, except for high pressure structural studies, the time-of-flight technique did not enjoy widespread use. One of the reasons is that, for a chopper-based diffractometer, the variation of the instrumental resolution with wavelength is opposite that which is most useful, i.e. the resolution is worst at short d spacings where the heaviest peak overlap occurs. This instrument property arises directly from the way the neutron pulses are formed. With a chopper, the width of the pulse in time-of-flight, t, is constant. Thus the resolution, $\Delta d/d = \Delta t/t$, is simply proportional to $1/d$.

In spite of this limitation, the time-of-flight technique can be used to achieve unusually high resolution by collecting the complete diffraction pattern in back scattering. The overall instrumental resolution function has the general form [Worlton et al 1976]:

$$R(d) = \Delta d/d = [(\Delta t/t)^2 + (\Delta\theta \cot\theta)^2 + (\Delta L/L)^2]^{1/2} \quad (2)$$

where θ is the scattering angle and L is the total path length from the point the pulses are formed to the sample and then to the detector. High resolution can be achieved in a straightforward way by placing the detector at 2θ approaching 180° and making the path length, L, long, which also lengthens the overall time-of-flight, t.

Steichele and Arnold [1973] demonstrated this concept with a high resolution, back-scattering time-of-flight diffractometer at the Garching reactor. The flight path was 145m long and utilized a neutron guide tube to maintain flux. Since a single mechanical chopper cannot produce a short pulse and then remain closed long enough for the neutrons to travel such a distance, multiple choppers were used to form the desired pulse and eliminate additional pulses that would otherwise lead to unwanted "frame overlap".

All of these early time-of-flight diffractometers employed a principle called time focusing [Carpenter 1967] to increase the usable detector area, and thus the count rate. The concept of time focusing is based on the fact that the variable one wishes to measure is actually the d spacing, d, not the time-of-flight, t. From Bragg's law,

$$\lambda = 2d \sin\theta, \quad (3)$$

and the de Broglie relation,

$$\lambda = h/mv = ht/mL, \quad (4)$$

where h is Planck's constant, m is the neutron mass, and v is the neutron velocity, one can immediately derive that

$$d = ht/(2mL \sin\theta), \quad (5)$$

and it becomes apparent that if the detectors are placed on a locus defined by

$$L \sin\theta = \text{constant}, \quad (6)$$

neutrons scattered at different angles from the same d spacing will be

detected at the same time-of-flight. Since L in equation (6) is the total path length, the desired detector arrangements are not physically realizable in all cases [Jorgensen & Rotella 1982, Jorgensen et al 1989a]. For example, if the incident flight path (source to sample) is much longer than the scattered flight path (sample to detector), as was the case for the high resolution instrument of Steichele and Arnold [1973], the multiple detectors can be placed on the time-focused locus only in back scattering (where the sin function is slowly varying).

TIME-OF-FLIGHT DIFFRACTOMETERS ON PULSED SOURCES

Many of the shortcomings associated with time-of-flight diffraction on reactor sources have been overcome by advanced instrument designs implemented on the pulsed neutron sources [Jorgensen & Rotella 1982, Jorgensen et al 1989a, Windsor 1981, Brown et al 1982]. The ability to form neutron pulses without a chopper provides several advantages. For example, the effective source area can be much larger than is straightforward to achieve with choppers. Additionally, the ratio of the pulse width to the time between pulses can be optimized.

At a pulsed source, the pulses are produced when a short burst of high energy neutrons produced by spallation in the target are moderated to thermal energies in a nearby moderator of comparably small dimensions, as shown in Figure 2 [Carpenter 1977, Carpenter et al 1978]. The initial high-energy neutron burst from the target is very short (less than 1 μs). The thermal neutron pulse duration, which is longer, depends on the moderator temperature and physical design and on the moderated neutron energy [Graham & Carpenter 1972]. One might estimate the pulse width as the distribution of times required for thermal neutrons to diffuse to the front surface of the moderator. Thus, higher energy neutrons exhibit shorter pulses. To first order, the pulse width, Δt, is proportional to wavelength, or equivalently, $\Delta t/t$ is nominally constant. Because of this, the undesirable resolution characteristics of chopper-based spectrometers are largely overcome. Furthermore, the time between pulses can be independently controlled to eliminate "frame overlap".

The limitations in achieving time focusing by detector placement have been overcome by a newly-developed method called electronic time focusing [Jorgensen et al 1989a]. The concept is straightforward. The detectors are placed in any convenient arrangement (for example, at a constant distance from the sample) and the data for each detector are separately time encoded. These individual detector data are then combined into a single histogram by computing the flight times for each detector that correspond to the same d spacing and then combining the

appropriate (constant d spacing) time channels. This focusing computation can either be done in real time (while the data are being collected) or later as a separate step. The real-time electronic focusing approach was used for the time-of-flight powder diffractometers at Argonne's Intense Pulsed Neutron Source [Jorgensen et al 1989a]. These instruments cover a wide range of d spacings by employing detectors at various angles between 12° and 157°.

A similar procedure has been used at the High Resolution Powder Diffractometer, HRPD, at ISIS for the past three years [David et al 1988]. At ISIS the diffraction patterns are collected with time bin widths that vary in a logarithmic manner as a function of time-of-flight (i.e. $\Delta t = \alpha t$). Typically, on HRPD and POLARIS (a medium-resolution, high-intensity powder diffractometer at ISIS) Δt (bin width) = $10^{-4}t$ and $10^{-3}t$ respectively. This logarithmic time-binning scheme has two significant advantages: first, over the whole diffraction pattern each Bragg peak is spanned by roughly the same number of time bins, and, second, time focusing can be achieved simply by including a channel-number offset for each detector in the computer memory, i.e., a simple register shift permits real-time detector focusing.

RIETVELD REFINEMENT WITH PULSED NEUTRON SOURCE DATA

Although the development of pulsed neutron sources motivated and, in some ways, made possible the development of advanced time-of-flight diffraction techniques, the characteristics of the pulsed source presented some challenging problems in applying the Rietveld method. The most important is the peak shape and its wavelength dependence. The neutron pulse from the moderator is highly asymmetric in time. The leading edge is very sharp, because the first neutrons to emerge are almost coincident with the high energy neutron pulse hitting the spallation target, while the trailing edge decays according to the moderator size and temperature. For most instrument designs, the other contributions to the resolution function are nominally Gaussian. Thus, the overall peak shape is the convolution of a Gaussian term with a function that describes the initial neutron pulse, and is highly asymmetric and non-Gaussian.

Windsor and Sinclair [1976] used a two-parameter asymmetric Gaussian peak profile to obtain reasonably good fits for nickel powder data from a pulsed source at the Harwell Linac. Later, analysis of high resolution nickel data on a 14m backscattering diffractometer required a more complex peak shape function based on a Gaussian leading edge and a second Gaussian trailing edge with an exponential tail [Windsor et al 1980, Cole & Windsor 1980]. An entirely empirical approach was

demonstrated by Mueller et al. who used a tabulated numerical peak shape function to fit data for Th_4D_{15} from the ZING-P pulsed neutron source at Argonne [Mueller et al 1977, Jorgensen et al 1978].

These first attempts at applying the Rietveld method to spallation pulsed neutron source data demonstrated the feasibility of the technique, but were difficult to apply and obscured the basic physics leading to the unusual peak shape. The first peak shape function that enjoyed widespread use in time-of-flight Rietveld codes was that proposed by Jorgensen et al [Jorgensen et al 1978, Carpenter et al 1975], based on a convolution of separate rising and falling exponentials that represented the time dependence of the initial neutron pulse with a symmetric Gaussian term that represented the other contributions to the peak shape. The integrals can be done in closed form and the resulting peak shape function has the form:

$$I(t) = \alpha\beta[\exp(u)\mathrm{erfc}(y) + \exp(v)\mathrm{erfc}(z)]/[2(\alpha+\beta)], \tag{7}$$

where $\mathrm{erfc}(y) = 1-\mathrm{erf}(y)$ and $\mathrm{erf}(y)$ is the error function, and

$$u = \alpha(\alpha\sigma^2 + 2t)/2, \qquad v = \beta(\beta\sigma^2 - 2t)/2, \tag{8}$$
$$y = (\alpha\sigma^2 + t)/(\sqrt{2}\sigma), \qquad z = (\beta\sigma^2 - t)/(\sqrt{2}\sigma).$$

α and β characterize the rising and falling exponentials used to model the time dependence of the neutron pulse (with respect to a reference time t^* that corresponds to the maximum of the pulse),

$$\exp(\alpha t^*),\ t^*<0 \quad \text{and} \quad \exp(\beta t^*),\ t^*>0, \tag{9}$$

and σ describes the width of the Gaussian component.

With α, β and σ as adjustable parameters, this function provided a precise fit to the observed peak shapes, as shown in Figure 3 [Jorgensen et al 1978, Carpenter et al 1975, Albinati & Willis 1982]. The incorporation of this peak shape function into a Rietveld code, however, required that the wavelength (or d spacing) dependence of α, β, and σ be specified. This information was obtained from diffraction data for standard samples and the required dependence empirically fitted to analytical functions by Von Dreele et al [1982] to produce the first widely used pulsed-source time-of-flight Rietveld code.

Subsequent codes are mostly based on this same peak shape function, sometimes with minor modifications, and have been very successful. However, a recent code written by Izumi et al. [1982] uses a more complex peak shape function, the Ikeda-Carpenter function [Ikeda &

Carpenter 1985], that provides an improved fit to the peak shapes at small d spacings or where cold moderators are used because it models more accurately the time dependence of the initial neutron pulse under such conditions. This peak shape and the related Robinson-Taylor-Carpenter peak shape described in the next section have proved to be successful in high resolution studies at ISIS.

THE PEAK SHAPE IN HIGH RESOLUTION TIME-OF-FLIGHT POWDER DIFFRACTION DATA

The Ikeda-Carpenter (IC) function [Ikeda & Carpenter 1985] represents the state-of-the-art description of the neutron pulse shape emanating from a moderator at a pulsed neutron source. It is a rather complicated function consisting of epithermal (slowing down) and thermal (storage term) components. The function is illustrated in Figure 4 along with another popular peak shape description ascribed to Robinson, Taylor and Carpenter (RTC). Although the Ikeda-Carpenter function more appropriately describes the short-wavelength epithermal region, both functions oversimplify the line shape function in the 'switching' region. However, for the purposes of profile fitting, these lines shapes are adequately precise.

The computation of the IC and RTC functions is easily tractable with modern day computers. However, with the advent of high resolution time-of-flight powder diffractometers, the folding of sample broadening contributions into the instrumental line shape must be accounted for. The most flexible method of tackling this problem is based on a Fourier transform algorithm. This method follows from an important property of Fourier transforms associated with the convolution of two (or more) functions.

Consider a peak shape, p(x), resulting from the convolution of instrumental, q(x), and sample, r(x), broadening contributions. Mathematically this is written as:

$$p(x) = \int_{-\infty}^{\infty} q(x')r(x-x')dx'. \qquad (10)$$

Symbolically we can write this as

$$p(x) = q(x) \star r(x). \qquad (11)$$

where $\star$ denotes convolution.

It may be shown [see, for example, Champeney 1973] that the corresponding Fourier transforms P(k), Q(k), and R(k) are simply related by the product equation

$$P(k) = Q(k)R(k). \tag{12}$$

For complete convolutions, the product rule for Fourier transforms also holds; i.e., if

$$p(x) = q_1(x)\star q_2(x)\star....\star q_n(x)\star r_1(x)\star r_2(x)\star....\star r_m(x), \tag{13}$$

then

$$P(k) = Q_1(k)Q_2(k)....Q_n(k)R_1(k)R_2(k)....R_m(k). \tag{14}$$

A good example of the success of the Fourier transform approach to peak shape description is provided by the study of oxygen loss in $YBa_2Cu_3O_{7-x}$ [David et al 1989]. $YBa_2Cu_3O_{7-x}$ possesses a wide range of stoichiometry for $x \approx 0$ (95K superconductor) to $x \approx 1$ (insulating antiferromagnet). Samples of nominal composition $x = 1$ were prepared by heating cold-pressed slabs of $YBa_2Cu_3O_{6.9}$ at 850°C in vacuum (10^{-4} Torr) for 12h. Diffraction data recorded on HRPD at ISIS indicated that the material had transformed to the anticipated tetragonal structure. Standard profile refinement was performed using a Voigt ⋆ double-exponential peak shape function. However, the attempts at refinement were only modestly successful because of a pronounced anisotropic, asymmetrical broadening associated with the c axis (Figure 5). Given that the c axis expands substantially on removal of oxygen, it was hypothesized that this broadening was caused by an oxygen gradient within the slab with the lowest oxygen content on the surface of the slab. Assuming linear variations of c versus oxygen stoichiometry and oxygen content versus depth into the slab, the effective scattering density for the resulting c-axis microstrain distribution may be expressed as a truncated quadratic equation, $y = 3t_\Delta^2/\eta^3$ for $0 < t_\Delta < \eta$ and $y = 0$ elsewhere, where η is the time range over which the scattering extends and t_Δ is the time-of-flight within this range. Note the η is a function of hkl, being maximum along c and zero for hk0 reflections. The precise formula is given by

$$\eta = t_0(\Delta c/c)(ld/c)^2, \tag{15}$$

where t_0 and d are the time-of-flight and d spacing associated with the hkl reflection, c and $\Delta c/c$ are, respectively, the c axis and fractional shift in c axis, and l is the third Miller index. Accordingly this additional

functional contribution was folded into the existing Voigt ⋆ double exponential function and Rietveld refinement performed. The improved fit is evident from a comparison of Figures 5 and 6. Chi-squared improves from 4.59 to 1.69: the weighted profile R-factor decreases from 14.2% to 8.5% against an expected R-factor of 6.6%. Most importantly, the refined average oxygen content changes from 6.038(8) to 6.075(5) with an estimated variation, from the width of the truncated quadratic function, of ~ 0.2 formula units of oxygen across the slab. This result not only highlights the complexity of peak shape that is necessary for successful Rietveld refinement of high resolution data, but also the care required in preparation of oxygen-deficient samples of $YBa_2Cu_3O_{7-x}$.

ANISOTROPIC LINE-BROADENING IN TIME-OF-FLIGHT POWDER DIFFRACTION DATA

Although of no particular benefit in standard Rietveld refinement, the roughly constant $\Delta d/d$ resolution of a time-of-flight powder diffractometer is particularly useful in the study of structural phase transitions and the analysis and separation of crystallite size and microstrain broadening. In the former case, the advantage of constant $\Delta d/d$ resolution rests in the fact that all orders of reflection are split by the same amount. With the large range of available d spacings it is not uncommon that splittings are observed in 3 or 4 orders of a given reflection. This permits a uniquely detailed description of structural distortions and pseudosymmetry. For example, two different measurements of the monoclinic angle of NiO at 90.05953(4)° and 90.06051(6)° on HRPD (ISIS) were accounted for by the differences in ambient temperature during the experiment (15°C and 23°C). In the case of size/strain effects, the excellent resolution at long d spacings permits the easy discrimination of size and strain effects. For crystallite size effects, it is easily shown that

$$\Delta d^* = \Delta d/d^2 \sim 1/P, \text{ where } (P = \text{crystallite size}), \quad (16)$$
$$\text{i.e., } \Delta d/d \sim d/P.$$

By contrast, for microstrain, $\langle\varepsilon\rangle$,

$$\langle\varepsilon\rangle = \Delta d/d = \Delta d^*/d^*. \quad (17)$$

Thus, peak widths vary linearly with time-of-flight for sample strain and the instrumental resolution function and quadratically for crystallite size effects. These contrasting width variations can be extremely pronounced when several orders of reflection are available.

With the advent of high resolution instrumentation such as the HRPD at ISIS, sample broadening in general dominates the intrinsic instrumental line shape. A modification, SAPS (Structure And Peak Shape refinement), of the Rietveld technique has been developed at ISIS to analyze peak broadening in a model-independent manner [David et al 1988]. Instead of accounting for the peak width by using a smooth functional variation that is parameterized in time-of-flight, the Gaussian and Lorentzian components of each peak may be separately refined. This results in a multi-parameter Rietveld problem. To ensure convergence, the widths of weak peaks may be constrained or the widths of closely overlapping peaks may be refined together. This approach often leads to substantial improvements in the Rietveld Refinement of high resolution data and has the distinct advantage that no assumptions are made about a particular line-broadening model.

A good example of the use of this Rietveld modification is provided by the analysis of data for $LaNbO_4$ collected on the HRPD at ISIS [David 1990]. High resolution neutron powder diffraction data were collected at a series of temperatures from a 1 cm^3 sample of $LaNbO_4$. Each run lasted for approximately 30 minutes. A small portion of the range of d spacings surveyed is shown in Figure 7. There is clear evidence of a structural phase transition. Indeed, the refined lattice parameters indicate a large monoclinic distortion that collapses in a mean-field manner at the transition temperature. The monoclinic shear angle is displayed in Figure 8.

Examination of the diffraction data collected at temperatures near the phase transition reveals significant broadening, particularly of some hk0 reflections. Standard Rietveld refinement with data obtained below 180°C and above 540°C proceeded routinely. However, at intermediate temperatures the refinements became progressively worse as the sample temperature approached that of the phase transition. Indeed, differences between diffraction patterns recorded at room temperature and the transition temperature were extremely pronounced. Using SAPS the peak widths were refined as independent variables. Structural parameters for $LaNbO_4$ that were unbiased by an imposed peak broadening model were thus obtained. A selection of the (Lorentzian) peak width components so refined are presented in Table 1.

These peak widths were then analyzed to determine the origin of the line broadening. Refinements at various temperatures revealed a pronounced temperature dependence that diverges around T_c. The anomalous Lorentzian broadening of the 220, $\bar{2}20$ and 112, $\bar{1}12$ reflections are displayed in Figure 9. The ratio of the slopes above and

below T_c is 2:1 within experiment error, as predicted by mean-field theory. The predominant nature of the Lorentzian broadening is consistent with microstrain effects described by a second rank tensor. Accordingly, anisotropic Lorentzian strain and particle size effects described by a second rank tensor formulation were added in convolution to the standard time-of-flight peak shape. The full-width-at-half-maxima formulae used were

$$\Gamma_{strain} = \xi d^2; \; \Gamma_{size} = \xi d^3 \tag{18}$$

where

$$\xi^2 = \Gamma_{11}h^2a^{*2} \; \Gamma_{22}k^2b^{*2} + \Gamma_{33}l^2c^{*2} +$$

$$2[\Gamma_{23}klb^*c^*\cos\alpha^* + \Gamma_{13}hla^*c^*\cos\beta^* + \Gamma_{12}hka^*b^*\cos\gamma^*]. \tag{19}$$

Rietveld refinement at a number of different temperatures indicated that the anisotropic broadening resulted from microstrain rather than size effects. This anomalous behavior is restricted to the ab plane; no extra broadening is associated with the c axis. The refined values shown in Table 2 clearly indicated microstrain anisotropy within the ab plane.

The anisotropic broadening of the Bragg peaks (microstrain) in $LaNbO_4$ may, as with the monoclinic lattice distortion (macrostrain), be described in terms of a second rank tensor. The principal axes of the ellipsoid representing the microstrain broadening is rotated by 21° from a*. This agrees to within experimental error (~ 2°) with the orientation of the principal axes of the spontaneous macrostrain hyperbola for all data sets collected between (T_c - 50°) and T_c.

The coincidence of the orientation of microstrain (obtained from line broadening considerations) and macrostrain (calculated from peak splittings associated with monoclinic symmetry) was unexpected and is at present unexplained, although the microstrain broadening is probably associated with crystal imperfections such as dislocations. For the purposes of the present paper it highlights the immense amount of detail that may be derived from the Rietveld refinement with powder diffraction data when sophisticated models for the peak broadening are employed.

WAVELENGTH DEPENDENT EFFECTS IN TIME-OF-FLIGHT RIETVELD REFINEMENT

The total number of neutrons, i.e., the integrated intensity, of a Bragg reflection measured in a time-of-flight powder diffraction experiment is given by Buras and Gerward [1975]:

$$I_{hkl} = \frac{I_o(\lambda)\, \mathcal{E}(\lambda)\lambda^4\, V_s A_{hkl}(\lambda)\, E_{hkl}(\lambda)\, j |F_{hkl}|^2 \cos\theta \Delta\theta}{4V_c^2 \sin^2\theta} \qquad (20)$$

The formula holds for the full Debye-Scherrer cone. The notation used is as follows:

$I_o(\lambda)$ = incident neutron flux at wavelength λ,
$\mathcal{E}(\lambda)$ = detector efficiency at wavelength λ,
$A_{hkl}(\lambda)$ = attenuation coefficient for reflection hkl,
$E_{hkl}(\lambda)$ = extinction coefficient for reflection hkl,
V_s = sample volume,
V_c = unit cell volume,
j = reflection multiplicity,
F_{hkl} = structure factor,
2θ = Bragg angle.

The first four symbols in the above list are wavelength dependent and must be correctly evaluated for a precise Rietveld refinement to be obtained. The product $I_o(\lambda)\mathcal{E}(\lambda)$ is usually determined by measuring the incoherent scattering from vanadium and accounting for inelasticity and multiple scattering effects. Although this is a non-trivial calculation that depends on the vanadium sample geometry (which should be identical to the sample configuration), cross-calibration with in-beam monitors is sufficient to allow normalization to proceed using corrected monitor spectra. The analysis of extinction and attenuation effects as a function of wavelength is more complex and requires detailed consideration. However, Sabine [1988] and Sabine, Von Dreele and Jorgensen [1988] have recently shown that severe extinction can be correctly modeled (if anisotropic) and, therefore, is not an impediment to time-of-flight Rietveld refinement. Similarly attenuation, (including absorption, self-attenuation, and multiple scattering) may be refined to good precision in most cases using a simplified attenuation description

[Sabine, this book].

The combined refinement of scale factor, temperature factors, attenuation, and extinction may lead to correlated or unstable Rietveld refinements. In refinements where accurate temperature factors are required, the experimental evaluation of sample attenuation using a combination of monitors before and after the sample is essential. For the case of a slab-shaped sample the sample attenuation may be shown, to a good approximation, to be given by the formula

$$A(\lambda) = [R^2(\lambda) - 1]/[2\ln(R(\lambda))] \qquad (21)$$

where $R(\lambda)$ is the ratio of neutron counts in the downstream and upstream monitors.

PRECISION AND ACCURACY WITH TIME-OF-FLIGHT RIETVELD REFINEMENT

The high resolution and large accessible range of d spacings (particularly short d spacings) in a time-of-flight powder diffraction measurement in principle permit the determination of atomic coordinates and temperature factors in moderately complex crystal structures with both high precision, i.e., small standard deviations, and high accuracy, i.e., agreement with the physically correct values (as established by independent measurements). Assuming a constant $\Delta d/d$ resolution, simple calculations show that the number of resolved peaks, N_R, in a time-of-flight powder diffraction pattern is of the order of

$$N_R = 1/[3(\Delta d/d)] \qquad (22)$$

Allowing a factor of ~7:1 for the ratio of the number of resolved peaks to structural parameters refined to high precision implies that for $(\Delta d/d) \sim 5 \times 10^{-4}$ (as obtained on the High Resolution Powder Diffractometer HRPD at ISIS) the number of potential structural parameters in a high-precision study is approximately 100. As a test of these assumptions, the crystal structure of deuterated benzene was investigated with the HRPD [ISIS Report 1989]. The recent single-crystal neutron structure refinement by Jeffrey et al [1987] and theoretical calculations by Filippini et al. [1989] provided rigorous tests for the powder data collected on HRPD.

Benzene, C_6H_6, is one of the most important organic molecules, forming the basic building unit of all aromatic compounds. Because of its central

role in organic chemistry, benzene has been extensively studied by numerous experimental and theoretical techniques. The simplicity of the chemical formula, C_6H_6, belies, however, the complexity of its crystal structure. As a result of a complex packing configuration, benzene adopts an orthorhombic structure, space group Pbca (Z = 2), with a moderately-sized unit cell (a = 7.3550 Å, b = 9.3709 Å, c = 6.6992 Å, V = 461.7 $Å^3$).

Benzene melts at 6°C. A powder sample was, therefore, prepared by grinding 5 cm^3 of deuterated benzene in a glove box under a cold nitrogen atmosphere. The sample was then loaded into a cylindrical vanadium can and rapidly cooled to liquid helium temperatures (4 K) to avoid problems with preferred orientation. Data were collected at the high resolution 2 m position ($\Delta d/d \sim 5 \times 10^{-4}$) on HRPD for approximately nine hours (174 μA-hr). The raw data were corrected for incident flux (using a vanadium calibration), and cryostat and sample attenuation. The last correction was derived from a measurement of the transmitted neutron flux and showed significant structure from multiple-scattering self-attenuation effects.

Rietveld refinement was performed with the powder diffraction package developed at RAL [David et al 1988] based upon the Cambridge Crystallography Subroutine Library. The data ranged in d spacing from 0.606 Å to 1.778 Å, consisted of 5382 points, and included 1040 reflections. Small impurity peaks were present in the diffraction pattern. They were caused, somewhat remarkably, by the vanadium sample can and cryostat heat shields, even though vanadium has a near-zero coherent neutron cross section. At present, these peaks have not been considered in the data analysis. With the use of a peak shape consisting of a double-exponential decay convoluted with a Voigt function (itself the convolution of Gaussian and a Lorentzian function) an excellent least-squares fit to the powder diffraction data was obtained as is shown in Figure 10. Perhaps most remarkable about this Rietveld refinement profile is the intricate detail of the data at small d spacing arising from the unusually high resolution of the HRPD. These data provide a graphic example of the large amount of information that can be obtained from powder diffraction data when a high-resolution diffractometer is employed and when the sample itself exhibits a narrow intrinsic Bragg peak width.

The refined structural parameters, including 18 atomic coordinates and 36 anisotropic temperature factors, are listed in Table 3. Table 3 also

lists bond lengths, uncorrected for libration, obtained in the present study and from the work of Jeffrey et al. [1987]. The agreement is good, with few statistically significant differences, these probably resulting from systematic errors in the powder diffraction data. Experimental and theoretically calculated anisotropic temperature factors are presented in Table 4. With the exception of the B_{22} temperature factors for three carbon atoms, there is a remarkable agreement between the temperature factors obtained from the HRPD powder data and from the single-crystal data.

The results obtained from Rietveld refinement with HRPD data are only marginally inferior to the best single crystal data. The two experimental techniques agree closely with each other, and both differ from the theoretical calculations [Fillipini & Gramaccioli 1989], particularly in the values obtained for the anisotropic temperature factors for the deuterium atoms. The powder diffraction experiment thus strongly supports the single crystal study and indicates that further improved theoretical calculations are required. The quality of these powder diffraction results represents the present state of the art at ISIS. Further improvements in normalization procedure and multiphase analysis are currently under development and should lead to a precision and accuracy in moderately complex structure determination that compare favorably with the best single crystal results.

SPECIAL SAMPLE ENVIRONMENTS

One of the natural advantages of the pulsed-source neutron diffraction technique is the ability to provide complete data at a fixed scattering angle. For the case of special sample environments, the angle can be chosen to provide the best possible collimation so that the sample can be probed with no unwanted scattering from the surroundings [Jorgensen 1988]. Although there are advantages for all types of special sample environments, the most import cases are those in which the sample containment vessel must be close to, or in contact with, the sample.

The clearest example of such a case is diffraction at high pressure, where the pressure cell, in fact, must support the sample. As was already mentioned, diffraction at high pressure was the first widespread application of the time-of-flight technique, using chopper-

based instruments at reactor sources. This work has continued at the pulsed neutron sources and, of course, has benefited from the improvements in both resolution and flux. Jorgensen has recently reviewed structural studies at high pressure using time-of-flight neutron powder diffraction [Jorgensen 1990]. The most important advance resulting from the high flux and resolution at the pulsed sources has been the ability to solve and then refine unknown structures from the powder diffraction data. For example, the structure of KNO_3-IV was solved by indexing the observed d spacings to obtain the unit cell, determining the space group from the observed extinctions, and then refining by the Rietveld method for a trial structure based on analogy to other structures in the literature [Worlton et al 1986]. The most complex structure solved to date from neutron powder diffraction data taken at high pressure is that of ND_4F-II [Lawson et al 1989]. The structure contains 24 molecules in a 1024 $Å^3$ hexagonal unit cell.

More recently, many of the newly discovered oxide superconductors have been studied by time-of-flight neutron powder diffraction as a function of pressure. Some of these compounds exhibit the largest pressure dependence of the superconducting transition temperature, dT_c/dP, observed for any superconductors [Murayama 1989]. The goal of neutron diffraction measurements at high pressure is to determine whether pressure-induced changes in particular structural features can be correlated with the changes in T_c. Such information provides an important test of models proposed to explain the behavior of these compounds in terms of the distribution of charge. The bond lengths determined from Rietveld refinement are used to determine the charge distribution. Figure 11 shows the Rietveld refinement profile of data for $YBa_2Cu_3O_{6.93}$ at a pressure of 0.58 GPa [Jorgensen et al 1990b]. The data were collected on the Special Environment Powder Diffractometer at Argonne's IPNS with the sample in a helium-gas pressure cell specially designed for time-of-flight diffraction. One of the most striking features of these data is the complete absence of any scattering from the pressure cell. This is achieved by incorporating neutron shielding embedded in the walls of the pressure cell to eliminate all scattered neutrons except those scattered from the sample at $2\theta=85°$-$95°$ [Jorgensen et al 1990b]. Using this technique, it is possible to achieve Rietveld refinements for samples in high pressure environments of a quality equal to that achieved under ambient conditions.

Another area in which the time-of-flight technique has had major impact is for high temperature diffraction. Here, for achieving high temperatures with small thermal gradients it is advantageous to have the walls of the furnace fairly close to the sample. Again, the ability to collect data at a fixed scattering angle (typically $2\theta = 90°$) is a clear advantage. Perhaps the most famous high temperature neutron diffraction experiments in recent years are the studies of oxide superconductors in which oxygen site occupancies varied over a wide range. In the case of $YBa_2Cu_3O_{7-x}$ these experiments must be done in atmospheres with controlled oxygen partial pressures [Jorgensen et al 1987, Jorgensen et al 1989b]. From the data, the site occupancies of particular oxygen sites are obtained by Rietveld refinement as shown in Figure 12. These high temperature in situ measurements are then correlated with the superconducting properties for oxygen-deficient $YBa_2Cu_3O_{7-x}$, which vary as a function of both the oxygen concentration and the ordering of oxygen atoms on the available sites [Jorgensen et al 1990].

FUTURE DEVELOPMENTS

Although remarkable advances in time-of-flight powder diffraction methods at pulsed neutron sources have occurred in recent years, these methods may be properly viewed as being in their infancy. The ultimate flux capabilities of the spallation pulsed neutron sources have not yet been reached. Based on presently known design concepts, one to two additional orders of magnitude in flux appears feasible [Lander & Emery 1985]. Clearly this will allow the design of yet another generation of sophisticated instrumentation. Many new instrument design concepts are already known, and are awaiting the opportunity to be tested. These future developments will undoubtedly include the extension of experimental capabilities to higher resolution, smaller samples, and more rapid data collection for real time measurements. At the same time, it is clear that the general concepts of Rietveld refinement, i.e., the concept that a calculated model of the diffraction data can be compared directly with the complete diffraction profile, will be expanded to allow access to the new information available in the data. In a single refinement with such data, one could expect to obtain not only the crystal structure parameters, but also such information as the parameters describing commensurate or incommensurate structural modulations [see, for example, Izumi, this book], the magnitude and direction of macrostrain and microstrain, parameters describing the texture, and the configurations of point and extended defects including

the local pair distributions that give rise to diffuse background scattering.

ACKNOWLEDGEMENTS

W. I. F. David is supported by the UK Science and Engineering Research Council. J. D. Jorgensen is supported by the U.S. Department of Energy, Office of Basic Energy Sciences, Division of Materials Sciences, under contract number W-31-109-ENG-38.

REFERENCES

Albinati A. and Willis B. T. M. 1982 J. Appl. Crystallogr. **15**, 361

Brown B. S., Carpenter J. M., Jorgensen J. D., Price D. L., and Kamitakahara W. 1982 in Novel Materials and Techniques in Condensed Matter, edited by G. W. Crabtree and P. Vashishta (North Holland, New York) pp 311-340

Buras B. and Gerward L. 1975 Acta Crystallogr. A **31**, 372

Carpenter J. M. 1967 Nucl. Instrum. Methods **47**, 179

Carpenter J. M. 1977 Nucl. Instrum. Methods **145**, 91

Carpenter J. M., Price D. L., and Swanson N. J. 1978 IPNS: A National Facility for Condensed Matter Research (Argonne National Laboratory Report No. ANL-78-88)

Carpenter J. M., Mueller M. H., Beyerlein R. A., Worlton T. G., Jorgensen J. D., Brun T. O., Skold K., Pelizzari C. A., Peterson S. W., Watanabe N., Kimura M., and Gunning J. E. 1975 in Proc. Neutron Diffraction Conf, Petten, Netherlands, 5-6 August 1975 (Reactor Centrum Nederland, RCN-234) pp 192-208

Cartz L. and Jorgensen J. D. 1981 J. Appl. Phys. **52**, 236

Cartz L., Srinivasa S. R., Riedner R. J., Jorgensen J. D., and Worlton T. G. 1979 J. Chem. Phys. **71**, 1718

Champeney D. C. 1973 Fourier Transforms and their Physical Applications, (Academic Press, London and New York)

Cole I. and Windsor C. G. 1980 Nucl. Instrum. Methods **171**, 107

David W. I. F. 1990 in Neutron Scattering for Materials Science, edited by S. M. Shapiro, S. C. Moss, and J. D. Jorgensen (Materials Research Society Symposium Proceedings, Vol. 156, Pittsburgh) pp. 41-54

David W. I. F., Akporiaye D. E., Ibberson R. M., and Wilson C. C. 1988 Rutherford Appleton Laboratory Report No. RAL-88-103

David W. I. F., Moze O. , Licci F., Bolzoni F., Cywinski R., and Kilcoyne S. 1989 Physica B **156 & 157**, 884

Decker D. L., Beyerlein R. A., Roult G., and Worlton T. G. 1974 Phys. Rev. B **10**, 3584

Fillipini G. and Gramaccioli C. M. 1989 Acta Crystallogr. A **45**, 261

Graham K. F. and Carpenter J. M. 1972 Nucl. Sci. Eng. **49**,418

Ikeda S. and Carpenter J. M. 1985 Nucl. Instrum. Methods A **239**, 536

ISIS Annual Report 1989 Rutherford Appleton Laboratory

Izumi F., Asano H., Murata H., and Watanabe N. 1982 J. Appl. Crystallogr. **20**, 581

Jeffrey G. A., Ruble J. R., McMullan R. K., and Pople J. A. 1987 Proc. R. Soc. Lond A **414**, 47

Jorgensen J. D. 1978 J. Appl. Phys. **49**, 5473

Jorgensen J. D. 1988 in Chemical Crystallography with Pulsed Neutrons and Synchrotron X-rays, edited by M. A. Carrondo and G. A. Jeffrey, NATO ASI Series C, Mathematical and Physical Sciences Vol. 221 (D.

Reidel Publishing Co., Dordrecht) pp 159-186
Jorgensen J. D. 1990 in High Pressure Science and Technology (Proc. 12th AIRAPT and 27th EHPRG International Conference, Paderborn, Germany, 17-21 July 1989), edited by W. B. Holzaphel and P. G. Johansen (Gordon and Breech, London) pp. 441-443; also published as High Pressure Research 4, 441 (1990).
Jorgensen J. D., Beno M. A., Hinks D. G., Soderholm L., Volin K. J., Hitterman R. L., Grace J. D., Schuller I. K., Segre C. U., Zhang K., and Kleefisch M. S. 1987 Phys. Rev. B **36**, 3608
Jorgensen J. D., Beyerlein R. A., Watanabe N., and Worlton T. G. 1984 J. Chem. Phys. **81**, 3211
Jorgensen J. D. and Clark J. B. 1980 Phys. Rev. B **22**, 6149
Jorgensen J. D., Faber J., Jr., Carpenter J. M., Crawford R. K., Haumann J. R., Hitterman R. L., Kleb R., Ostrowski G. E., Rotella F. J., and Worlton T. G. 1989 J. Appl. Crystallogr. **22**, 321
Jorgensen J. D., Johnson D. H., Mueller M. H., Peterson S. W., Worlton T. G., and Von Dreele R. B. 1978 in Proc Conf. on Diffraction Profile Analysis, (Cracow, Poland, 14-15 August 1978) pp 20-22
Jorgensen J. D., Pei Shiyou, Lightfoot P., Hinks D. G., Veal B. W., Dabrowski B., Paulikas A. P., and Kleb R. 1990b Physica C (in press)
Jorgensen J. D. and Rotella F. J. 1982 J. Appl. Crystallogr. **15**, 27
Jorgensen J. D., Shaked H., Hinks D. G., Dabrowski B., Veal B. W., Paulikas A. P., Nowicki L. J., Crabtree G. W., Kwok W. K., Nunez L. H., and Claus H. 1989 Physica C **153-155**, 578
Jorgensen J. D., Veal B. W., Paulikas A. P., Nowicki L. J., Crabtree G. W., Claus H., and Kwok W. K. 1990 Phys. Rev. B **41**, 1863
Jorgensen J. D., Worlton T. G., and Jamieson J. C. 1978 Phys. Rev. B **17**, 2212
Lander G. H. and Emery V. J. 1985 Nucl. Instrum. Methods in Phys. Res. B **12**, 525
Lawson A. C., Roof R. B., Jorgensen J. D., Morosin B., and Schirber J. E. 1989 Acta Crystallogr. B **45**, 212
Mueller M. H., Beyerlein R. A., Jorgensen J. D., Brun T. O., Satterthwaite C. B., and Caton R. 1977 J. Appl. Crystallogr. **10**, 79
Murayama C., Mori N., Yomo S., Takagi H., Uchida S., and Tokura Y. 1989 Nature 339, 293
Rietveld H. M. 1969 J. Appl Crystallogr. **2**, 65
Sabine T. M. 1988 Acta Crystallogr. A **44**, 368
Sabine T. M., Von Dreele R. B., and Jorgensen J.-E. 1988 Acta Crystallogr. A **44**, 374
Steichele E. and Arnold P. 1973 Phys. Lett. A **44**, 165
Von Dreele R. B., Jorgensen J. D., and Windsor C. G. 1982 J. Appl. Crystallogr. **15**, 581
Windsor C. G. 1981 Pulsed Neutron Scattering (J. Wiley, New York-Toronto)

Windsor C. G., Bunce L. J., Borcherds P. H., Cole I., Fitzmaurice M., Johnson D. A. G., and Sinclair R. N. 1980 Nucl. Instrum. Methods **171**, 107

Windsor C. G. and Sinclair R. N. 1976 Acta Crystallogr. A **32**, 395

Worlton T. G. and Beyerlein R. A. 1975 Phys. Rev. B **12**, 1899

Worlton T. G., Decker D. L., Jorgensen J. D., and Kleb R. 1986 Physica B **136**, 503

Worlton T. G., Jorgensen J. D., Beyerlein R. A., and Decker D. L. 1976 Nucl. Instrum. Methods **137**, 331

FIGURE CAPTIONS

Fig. 1. Comparison of a measured diffraction peak for the chopper-based time-of-flight diffractometer at Argonne's CP-5 research reactor with a calculated Gaussian.

Fig. 2. Arrangement of the spallation target and moderators of the Intense Pulsed Source Neutron Source at Argonne National Laboratory (from Carpenter 1977, Carpenter et al 1978). High energy protons from the accelerator strike a cylindrical uranium target. The high energy neutrons thus produced in the target by spallation are moderated to lower energies (typically room temperature or below) in three hydrogenous moderators (A, B, and C) surrounding the target. Because of the relatively small dimensions of the moderators, a fraction of the neutrons in the final beam are undermoderated (i.e., possess energies higher than the moderator temperature). Neutron instruments view the surfaces of these moderators.

Fig. 3. Comparison of the 211 Bragg peak of iron, measured at Argonne's ZING-P spallation neutron source, with the calculated function of equation (7). (From Carpenter et al 1975, Jorgensen et al 1978).

Fig. 4. Schematic illustration of the functions that are convoluted to produce the Ikeda-Carpenter and Robinson-Taylor-Carpenter time-of-flight peak-shape functions.

Fig. 5. Observed and calculated profiles for a portion of the time-of-flight powder diffraction data for $YBa_2Cu_3O_{7-x}$ The isotropic line-shape model gives a poor fit, particularly for 001 reflections.

Fig. 6. Observed and calculated profiles for a portion of the time-of-flight powder diffraction of $YBa_2Cu_3O_{7-x}$. The line-shape model containing the convoluted anisotropic truncated quadratic function (see text) gives an excellent profile fit for all reflections.

Fig. 7. Diffraction patterns from a 1 cm^3 sample of $LaNbO_4$ recorded as a function of temperature. The peak splitting associated with the ferroelastic phase transition is evident.

Fig. 8. The variation of the monoclinic angle of $LaNbO_4$ as a function of temperature. Least square fitting confirms a mean-field behavior and a transition temperature of 483.0(1) °C.

Fig. 9. Refinement of individual peak widths for $LaNbO_4$ reveals a pronounced temperature dependence that diverges around the phase transition temperature, T_c. The distinction between 220 and $\bar{2}20$ (similarly, 112 and $1\bar{1}2$) peak widths is consistent with strain effects described by a second rank tensor.

Fig. 10. The final Rietveld refinement profile for data from benzene obtained on the HRPD at ISIS. The first four frames show the fit for d spacings from 0.5 to 2.0 Å. The final two frames show the fit for the range 0.68 to 0.78 Å on an expanded scale in order to better illustrate complexity of the data and the quality of the fit at small d spacings. Tick marks at the top of each plot indicate the positions of the Bragg reflections. A difference curve (observed minus calculated) plotted in units of the statistical uncertainty, σ, (square root of the number of counts) is plotted at the bottom. The dotted lines in the difference curves are at $+/-3\sigma$.

Fig. 11. Rietveld refinement profile for $YBa_2Cu_3O_{6.93}$ at 0.58 GPa in a helium-gas pressure cell. Scattering from the aluminum pressure cell is completely eliminated by incorporating neutron shielding in the walls of the cell in order to restrict the scattered beam to neutrons scattered from the sample at $2\theta = 85°$-$95°$. [From Jorgensen et al 1990b]

Fig. 12. Site occupancies of three of the oxygen sites in $YBa_2Cu_3O_{7-x}$ versus oxygen partial pressure at a constant temperature of 490°C. The site occupancies are obtained from Rietveld refinement of neutron powder diffraction data taken in situ in a flowing atmosphere. An orthorhombic-to-tetragonal transition occurs where the occupancies of the (0,1/2,0) and 1/2,0,0) sites meet. In the tetragonal phase these two sites are symmetry equivalent. (From Jorgensen et al 1989b).

TABLE 1.

Part of one of the output files from SAPS from the refinement with data for $LaNbO_4$ near the phase transition. The Table contains Miller indices, hkl, along with peak intensities, I, and standard deviations, $\sigma(I)$. If $I/\sigma(I)$ is greater than a predetermined value (12 in this particular case), peak widths are refined. For $I/\sigma(I) < 12$, peak widths are fixed (note zero standard deviations for some Γ). In this example the usual TOF functional form for σ was refined, All individual Gaussian widths were fixed.

h	k	l	I	$\sigma(I)$	Γ	$\sigma(\Gamma)$	σ	$\sigma(\sigma)$
0	1	5	663.8	20.5	25.3	3.9	51.8	0.0
1	0	5	540.2	20.6	43.1	5.3	51.9	0.0
-1	1	4	3646.5	37.8	49.7	1.7	55.9	0.0
1	1	4	3460.5	38.5	45.5	1.7	56.2	0.0
-1	2	1	715.1	24.2	112.5	8.5	56.7	0.0
-2	1	1	2443.0	31.0	40.7	2.1	57.1	0.0
1	2	1	2192.0	28.3	38.5	2.2	57.3	0.0
2	1	1	836.2	26.5	97.4	6.6	57.7	0.0
0	2	2	461.3	29.5	89.7	10.3	59.0	0.0
2	0	2	579.9	30.7	58.2	6.5	59.6	0.0
0	2	0	10.3	35.4	42.2	0.0	64.9	0.0
-2	0	0	0.7	35.7	42.8	0.0	65.8	0.0
0	0	4	121.4	43.7	45.9	0.0	70.6	0.0
0	1	3	361.6	45.4	49.6	0.0	76.2	0.0
1	0	3	303.1	30.3	49.8	0.0	76.5	0.0
-1	1	2	9352.3	89.6	114.4	2.7	77.0	0.0
1	1	2	10061.0	98.0	93.5	2.3	77.7	0.0

TABLE 2.

Refined anisotropic strain broadening terms for $LaNbO_4$ versus temperature.

T(°C)	Γ_{11}	Γ_{22}	Γ_{12}
240	205(15	402(20)	600(300)
270	198(15)	366(20)	900(300)
300	183(15)	392(20)	1600(300)
330	227(20)	378(20)	1500(300)
360	190(15)	447(25)	2500(400)
380	214(20)	462(25)	2300(400)
400	257(20)	417(25)	2600(500)
420	266(20)	598(30)	3900(600)
450	400(25)	676(30)	6500(1000)
460	460(40)	770(40)	8700(1500)
470	840(40)	1320(50)	15300(3000)
480	2200(200)	3800(250)	36000(5000)

TABLE 3.

Refined structural parameters for benzene from neutron powder diffraction data collected on the HRPD. Space group Pbca, Z = 2, molecular symmetry = $\bar{1}$, a = 7.3551(3) Å, b = 9.3712(4), c = 6.6994 Å, V = 461.76 Å^3

Atom	x / a	y / b	z/c	B_{iso} (x 10^{-4}Å^2)
C1	-0.06120(15)	0.14123(10	-0.00519(20)	68(6)
C2	-0.14023(15)	0.04469(10)	0.12722(15)	66(6)
C3	-0.07770(15)	-0.09689(12)	0.13264(20)	77(6)
D1	-0.10853(15)	0.25050(15)	-0.01187(25)	202(9)
D2	-0.24908(20)	0.07682(15)	0.22600(20)	202(9)
D3	-0.13821(20)	-0.17136(15)	0.23703(20)	203(9)

R_p = 13.2%, R_{wp} = 15.7%, R_{exp} = 10.8%, χ^2 = 2.1 (usual R-factor notation)

Benzene: Bond-lengths (4K) (uncorrected for libration)

C1-C2 = 1.3940(20) Å	C1-D1 = 1.0825(30) Å
C2-C3 = 1.4047(30) Å	C2-D2 = 1.0815(30) Å
C1-C3 = 1.3948(20) Å	C3-D3 = 1.0836(25) Å
mean = 1.3978(15) Å	mean = 1.0825(20) Å

Single crystal neutron diffraction (15K) (after Jeffrey et al. [1987])

C1-C2 = 1.3969(7) Å	C1-D1 = 1.0879(9) Å
C2-C3 = 1.3970(8) Å	C2-D2 = 1.0869(9) Å
C1-C3 = 1.3976(7) Å	C3-D3 = 1.0843(8) Å
mean = 1.3972(5) Å	mean = 1.0864(7) Å

TABLE 4.

Anisotropic temperature factors ($x10^4 Å^2$) for benzene at low temperatures

Lines 1 and 2: Harmonic lattice-dynamical calculation at 15K and 0K respectively [Fillipini & Gramaccioli 1989].
Line 3: Neutron single crystal diffraction data (15K) [Jeffrey et al 1987].
Line 4: Neutron powder diffraction data (4.2K) [ISIS Report 1989]

Atom	B_{11}	B_{22}	B_{33}	B_{23}	B_{13}	B_{12}
C1	90	66	89	3	7	0
	77	58	77	3	0	7
	79(2)	67(2)	88(2)	4(1)	7(2)	6(2)
	77(7)	42(6)	87(7)	1(5)	5(5)	-3(4)
C2	84	87	82	-2	17	6
	71	79	70	-2	17	9
	74(2)	81(2)	79(2)	0(2)	17(2)	9(2)
	71(7)	58(7)	68(6)	9(4)	26(5)	12(4)
C3	86	79	82	10	11	6
	73	72	70	10	11	-5
	81(2)	75(2)	82(2)	10(1)	14(2)	-3(2)
	83(7)	57(7)	92(7)	0(5)	18(5)	-1(4)
D1	216	173	212	11	39	38
	222	165	199	11	39	38
	224(3)	114(2)	239(3)	12(2)	25(2)	46(2)
	218(8)	121(7)	267(9)	19(5)	22(6)	31(5)
D2	184	226	215	5	56	56
	170	217	202	5	55	56
	183(2)	204(3)	208(3)	-8(2)	88(2)	35(2)
	170(8)	212(8)	225(9)	-2(6)	120(6)	33(5)
D3	228	208	171	60	37	-2
	215	199	158	59	36	-1
	214(3)	171(2)	199(3)	58(2)	61(2)	-18(4)
	241(9)	155(8)	214(8)	75(6)	66(7)	-20(5)

Fig 1

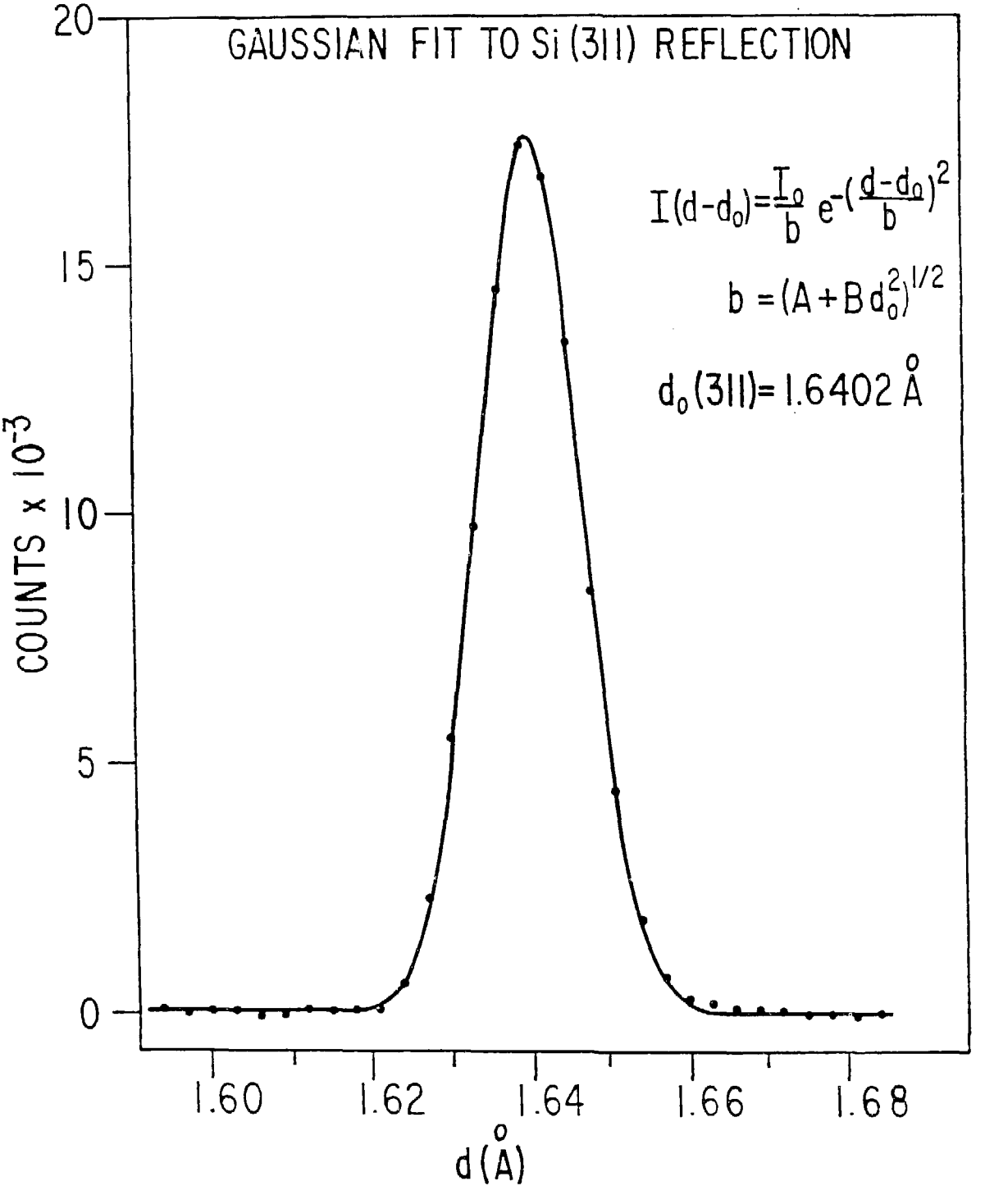
GAUSSIAN FIT TO Si (311) REFLECTION
$I(d-d_0)=\frac{I_0}{b}e^{-\left(\frac{d-d_0}{b}\right)^2}$
$b=(A+Bd_0^2)^{1/2}$
$d_0(311)=1.6402\,\text{Å}$
COUNTS x 10^{-3}
20
15
10
5
0
1.60
1.62
1.64
1.66
1.68
d(Å)

Fig 2

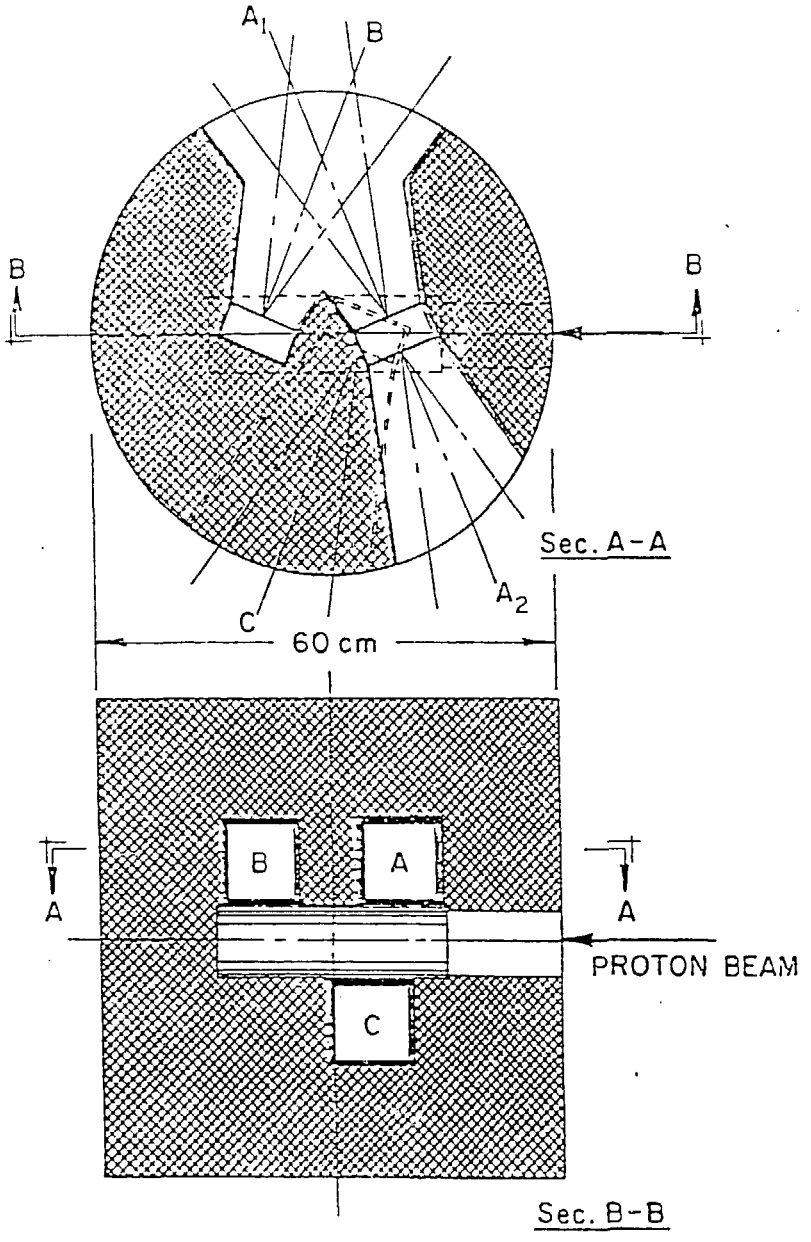

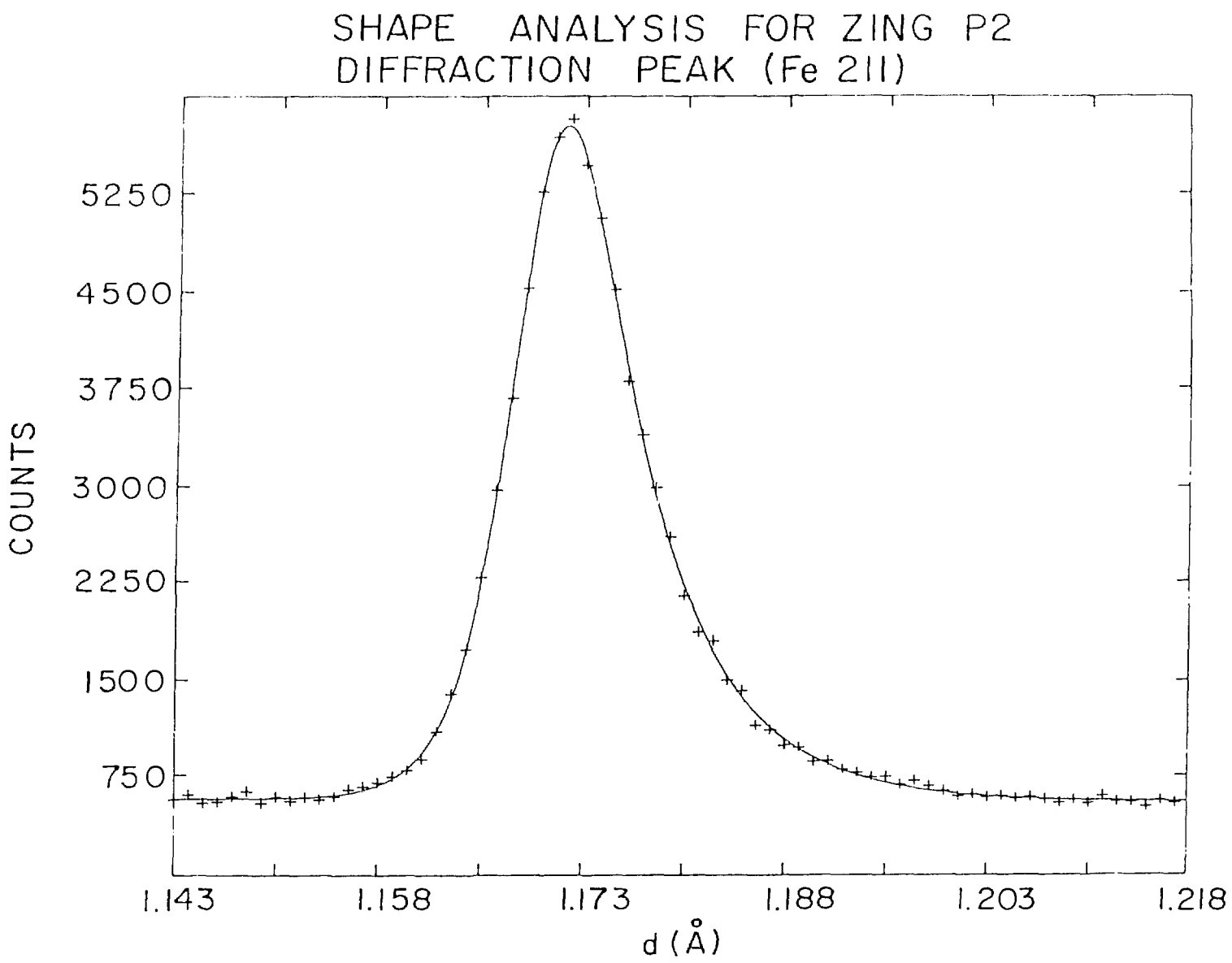
SHAPE ANALYSIS FOR ZING P2
DIFFRACTION PEAK (Fe 211)
COUNTS
5250
4500
3750
3000
2250
1500
750
1.143
1.158
1.173
1.188
1.203
1.218
d (Å)

Fig 3

Ikeda-Carpenter

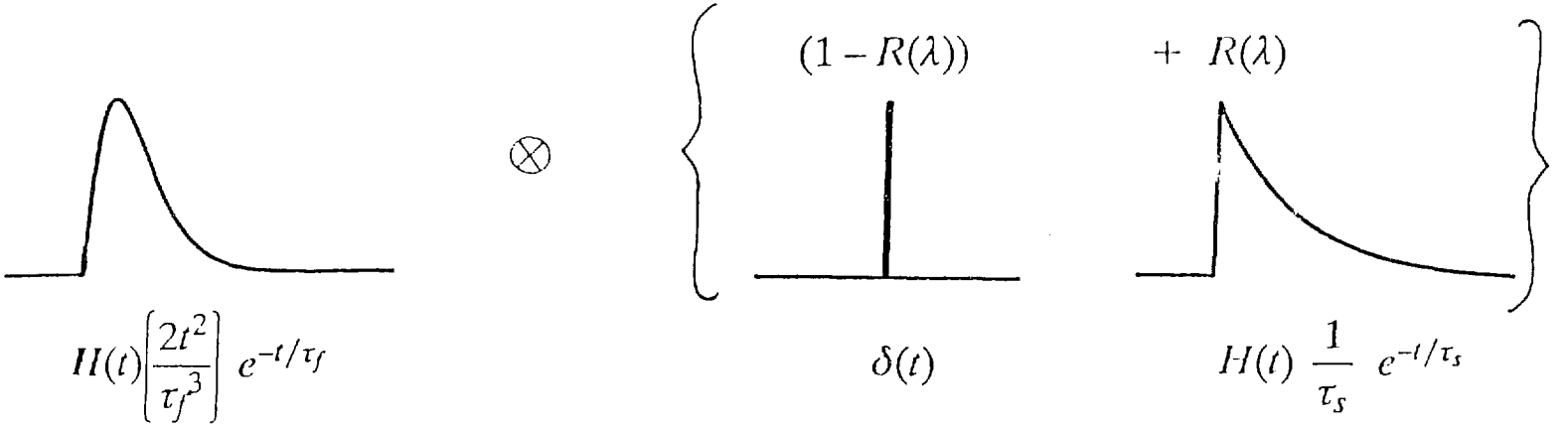

Robinson-Taylor-Carpenter

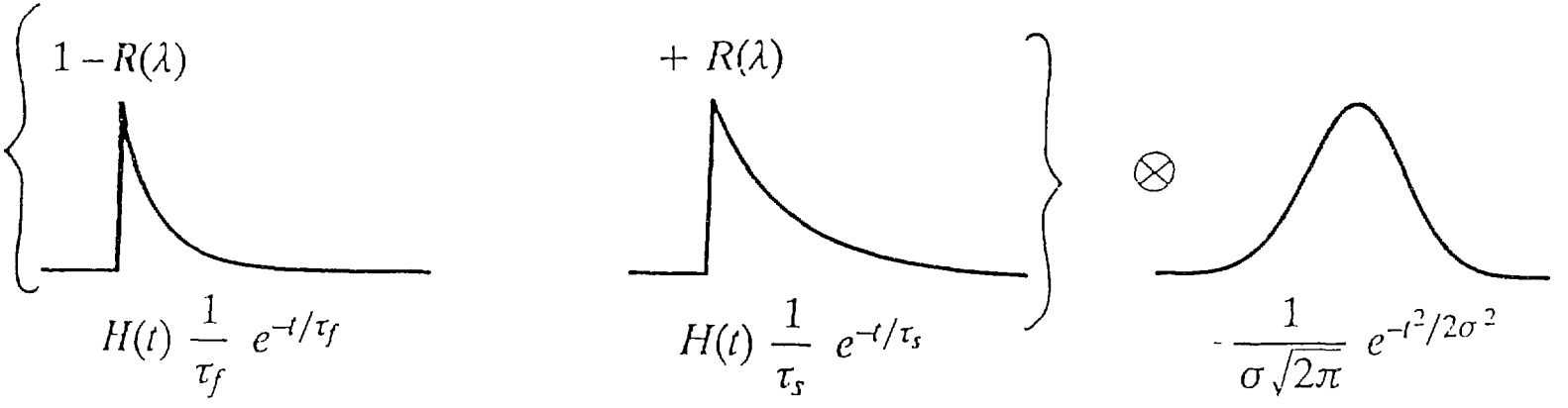

Fig 4

Fig 5

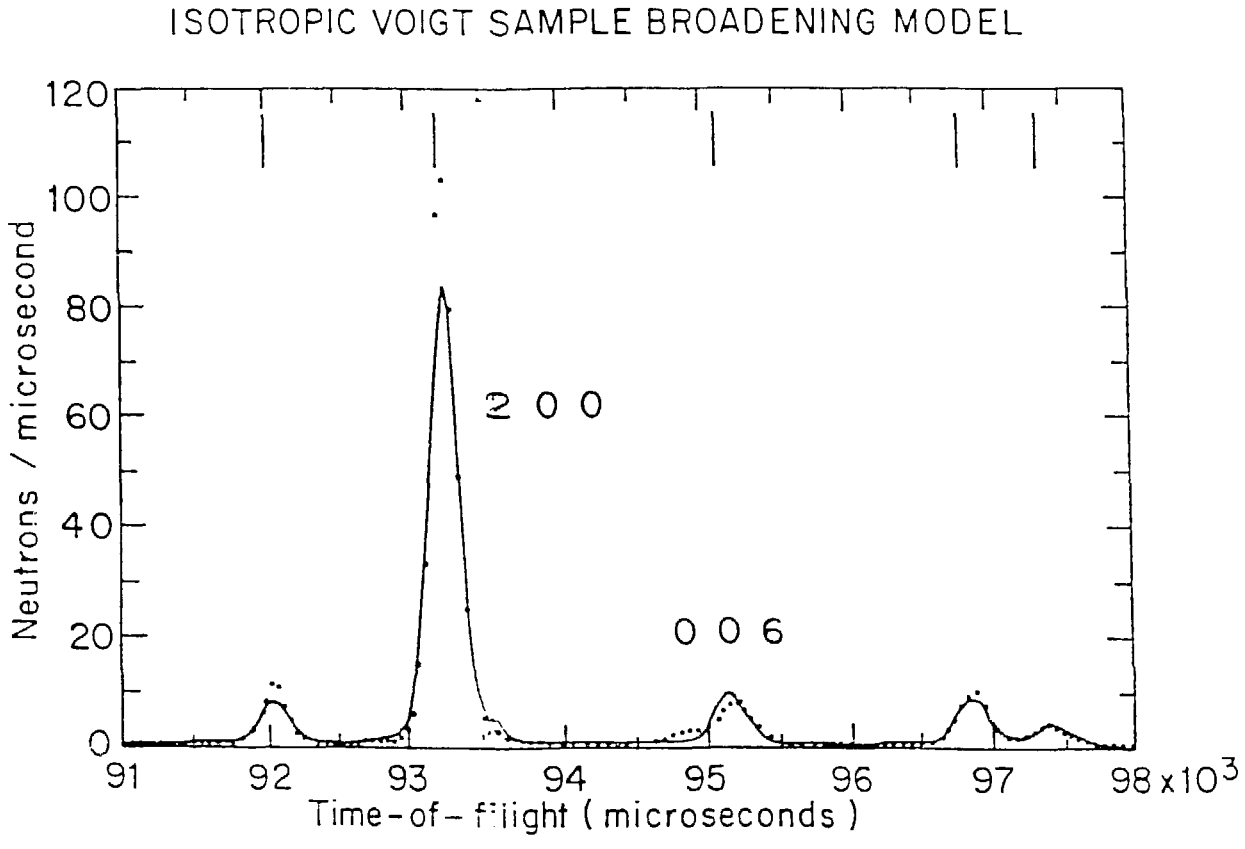
ISOTROPIC VOIGT SAMPLE BROADENING MODEL
120
100
80
60
40
20
0
Neutrons / microsecond
2 0 0
0 0 6
91
92
93
94
95
96
97
98 x10^3
Time-of-flight (microseconds)

Fig 6

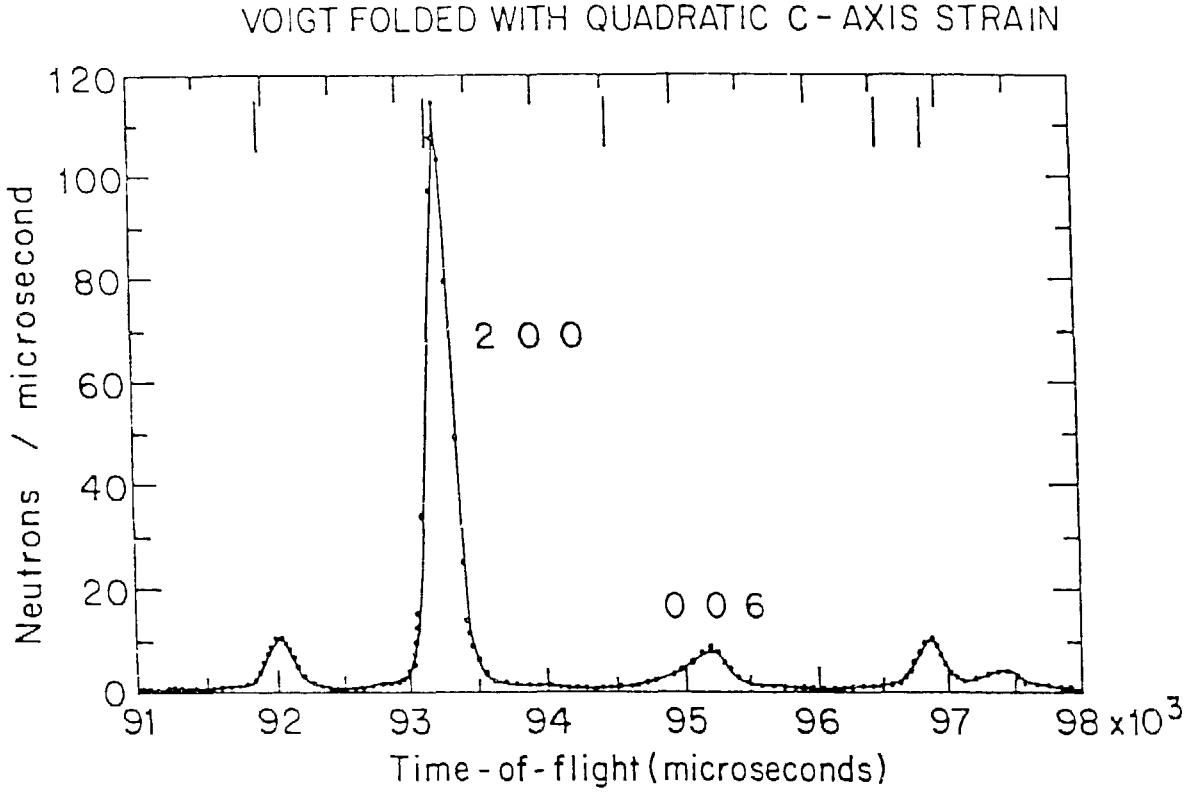
VOIGT FOLDED WITH QUADRATIC C-AXIS STRAIN
Neutrons / microsecond
120
100
80
60
40
20
0
2 0 0
0 0 6
91
92
93
94
95
96
97
98 x10^3
Time-of-flight (microseconds)

Fig 7

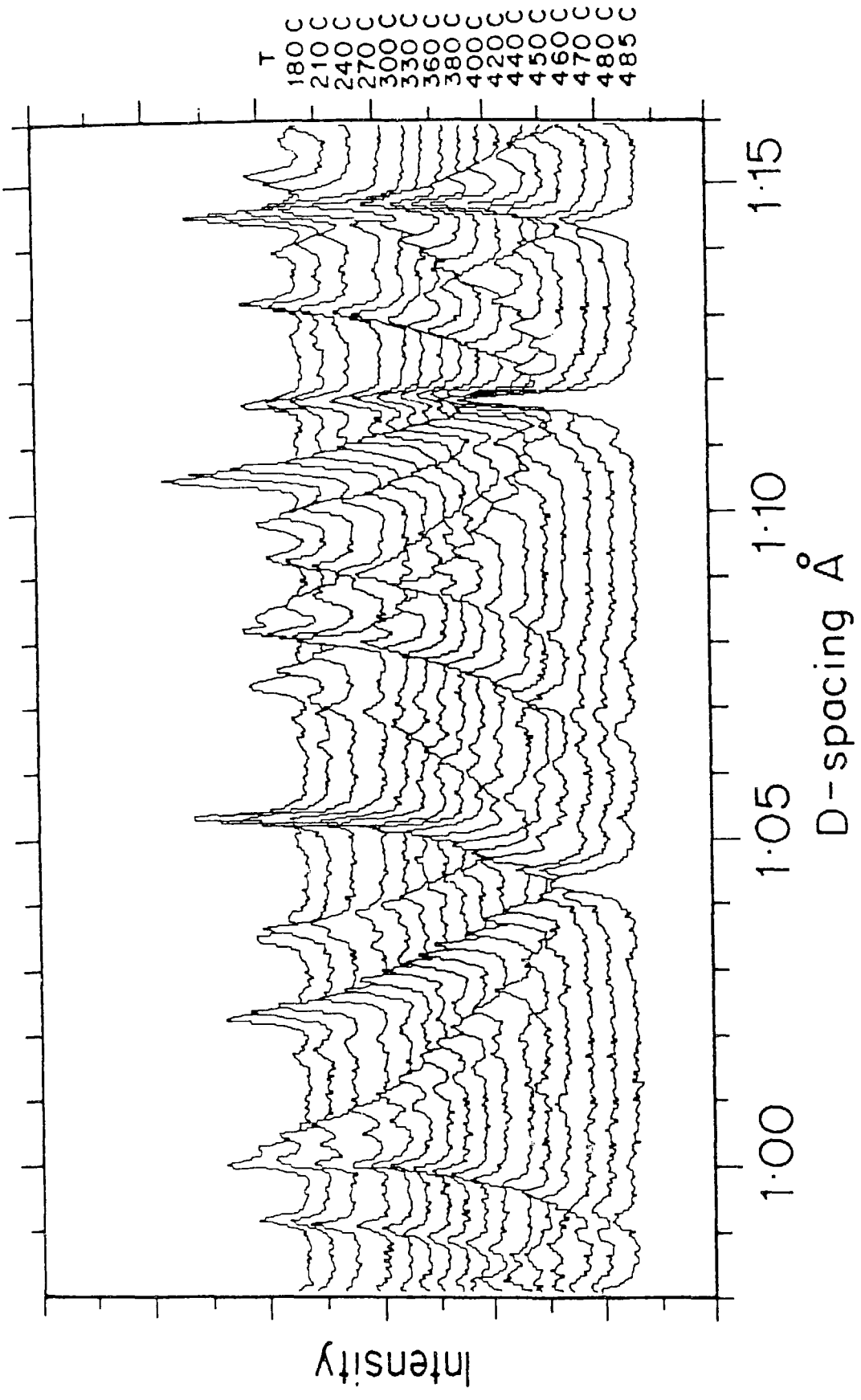
T
180 C
210 C
240 C
270 C
300 C
330 C
360 C
380 C
400 C
420 C
440 C
450 C
460 C
470 C
480 C
485 C
Intensity
1·00
1·05
1·10
1·15
D-spacing Å

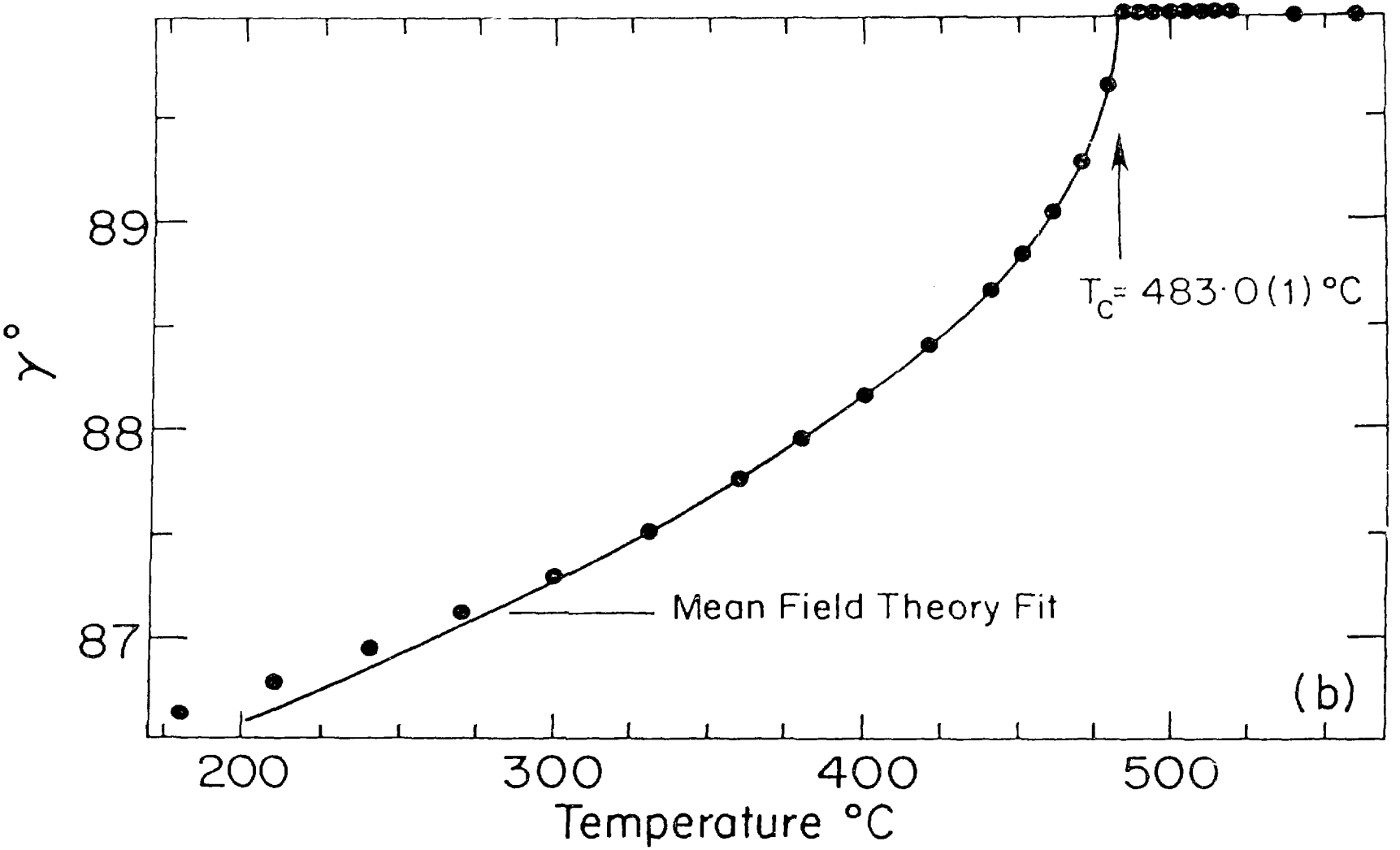
89
88
87
γ°
200
300
400
500
Temperature °C
T_C = 483·0(1) °C
Mean Field Theory Fit
(b)

Fig 8

Fig 9

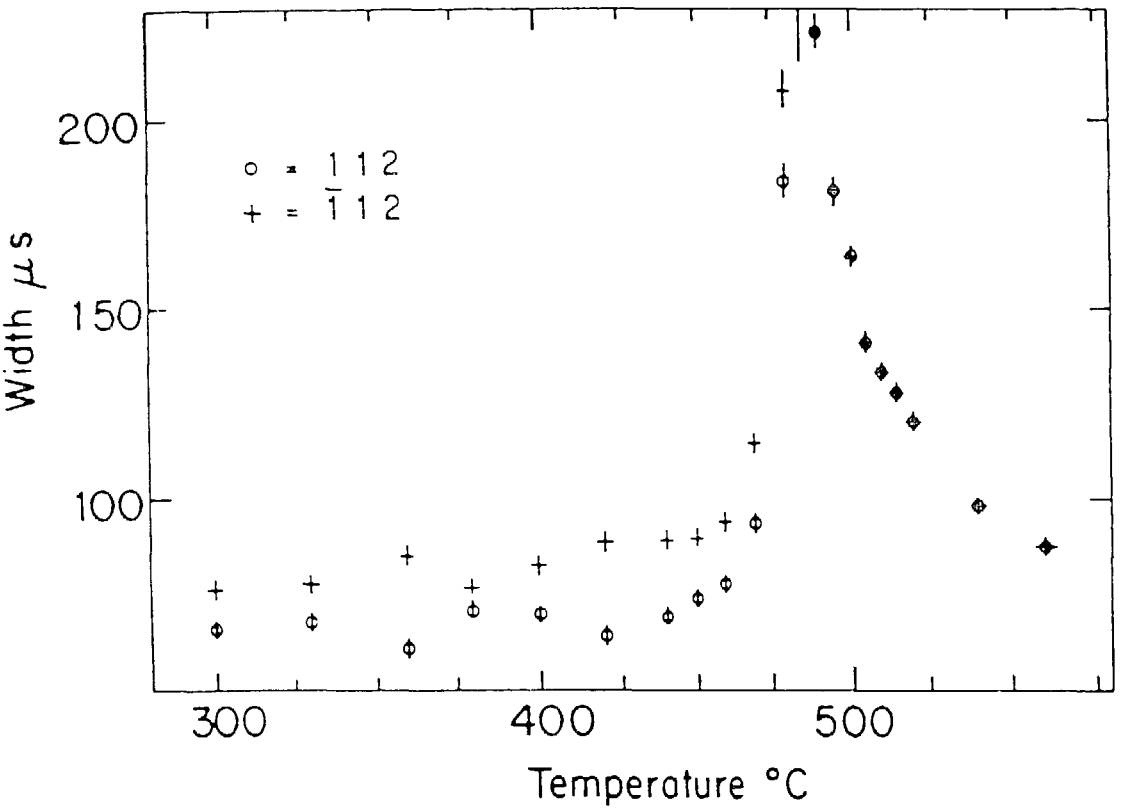
200
150
100
Width μs
o = 1 1 2
+ = $\bar{1}$ 1 2
300
400
500
Temperature °C

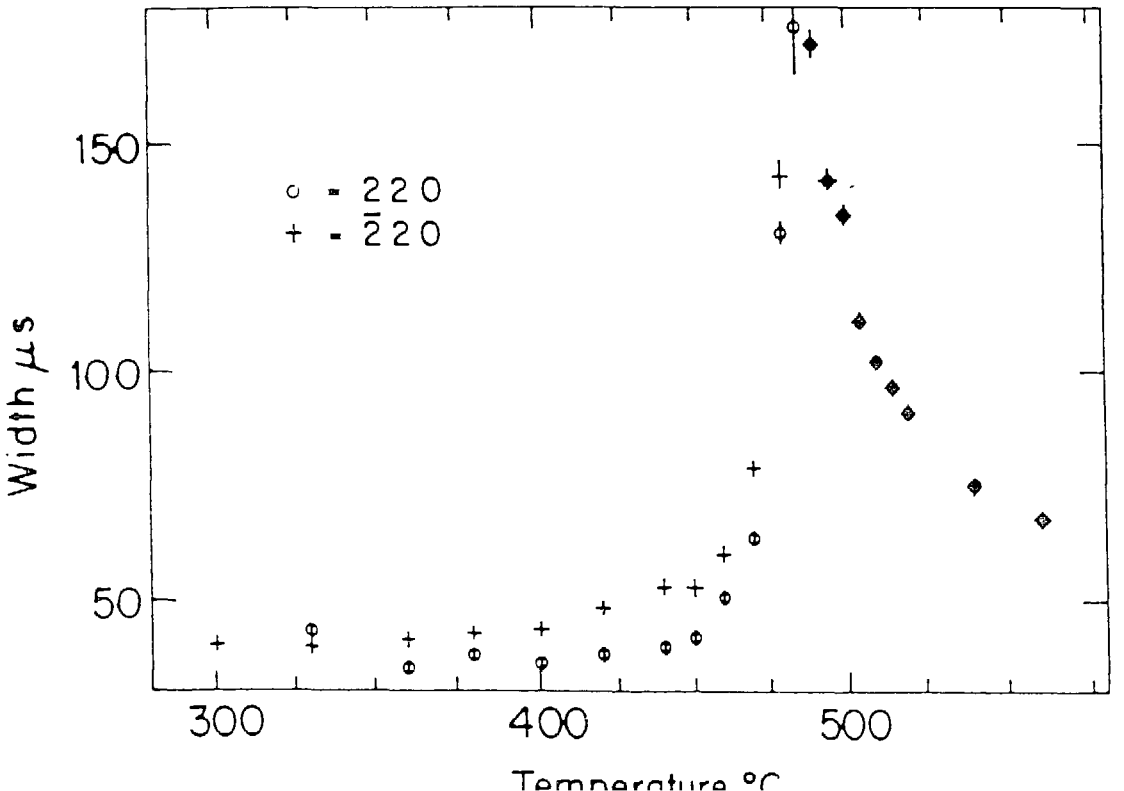
150
100
50
Width μs
o = 2 2 0
+ = $\bar{2}$ 2 0
300
400
500
Temperature °C

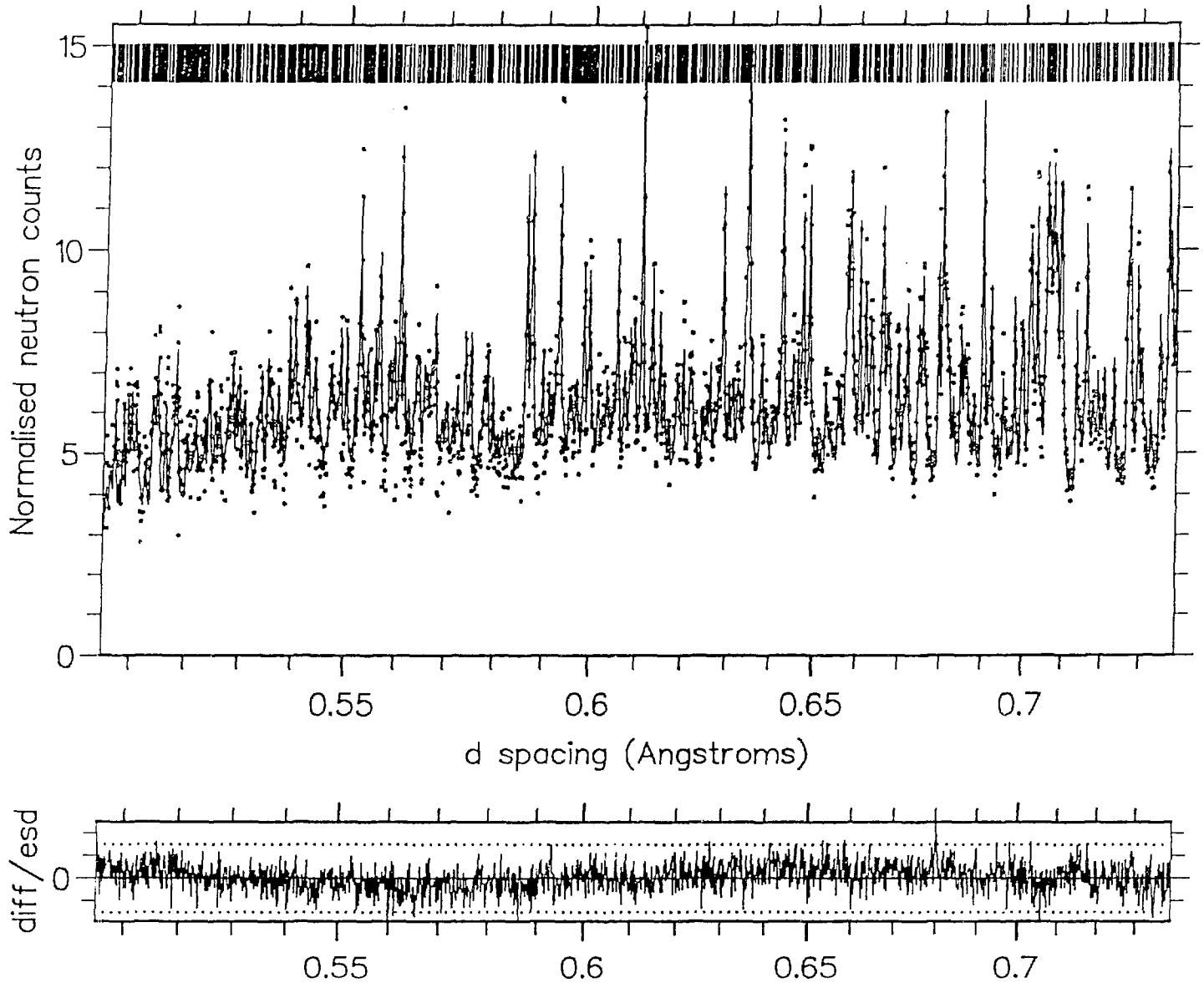
15
10
5
0
Normalised neutron counts
0.55
0.6
0.65
0.7
d spacing (Angstroms)
diff/esd
0
0.55
0.6
0.65
0.7

Fig 10(a)

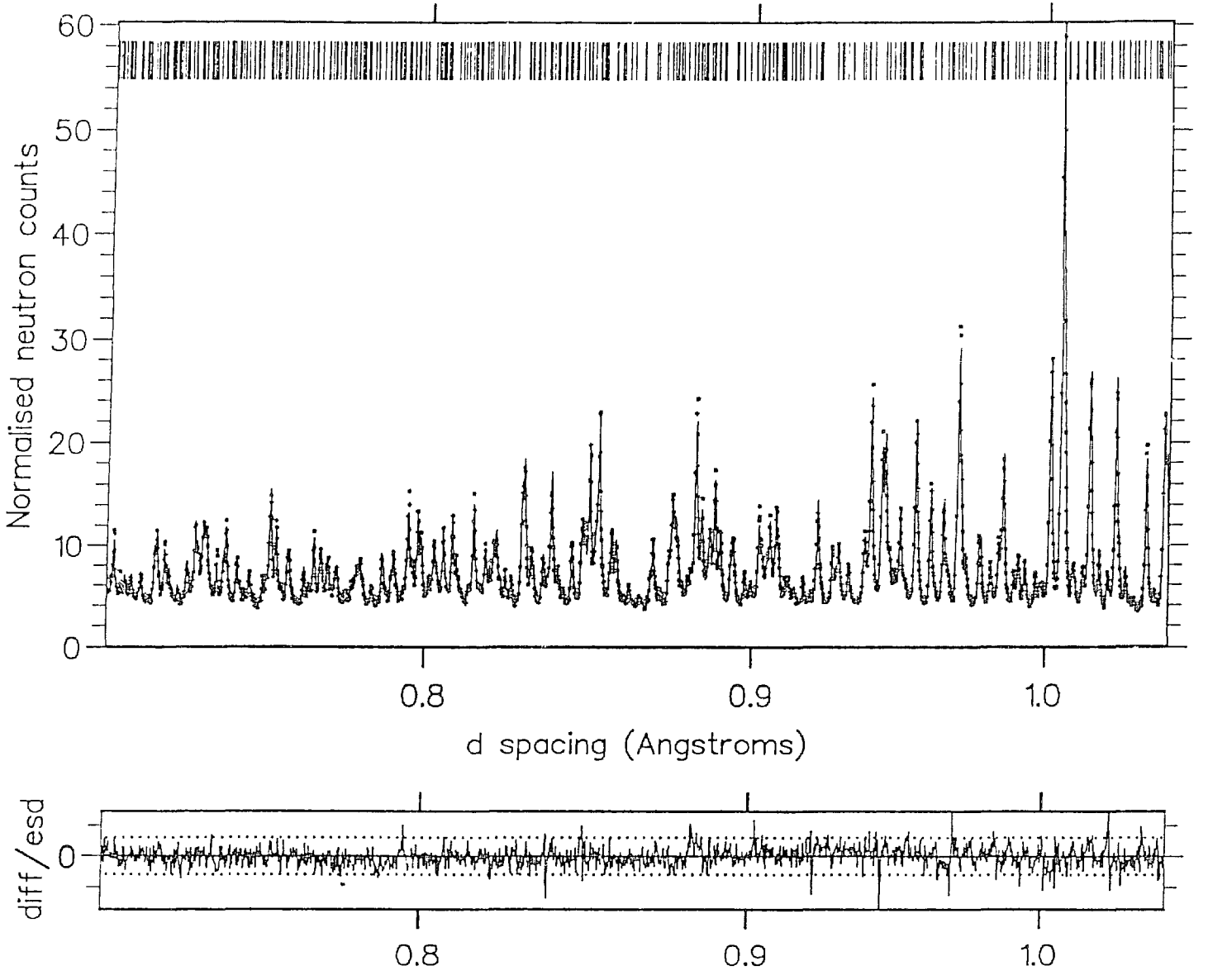
60
50
40
30
20
10
0
Normalised neutron counts
0.8
0.9
1.0
d spacing (Angstroms)
diff/esd
0
0.8
0.9
1.0

Fig 10(b)

Fig 10(c)

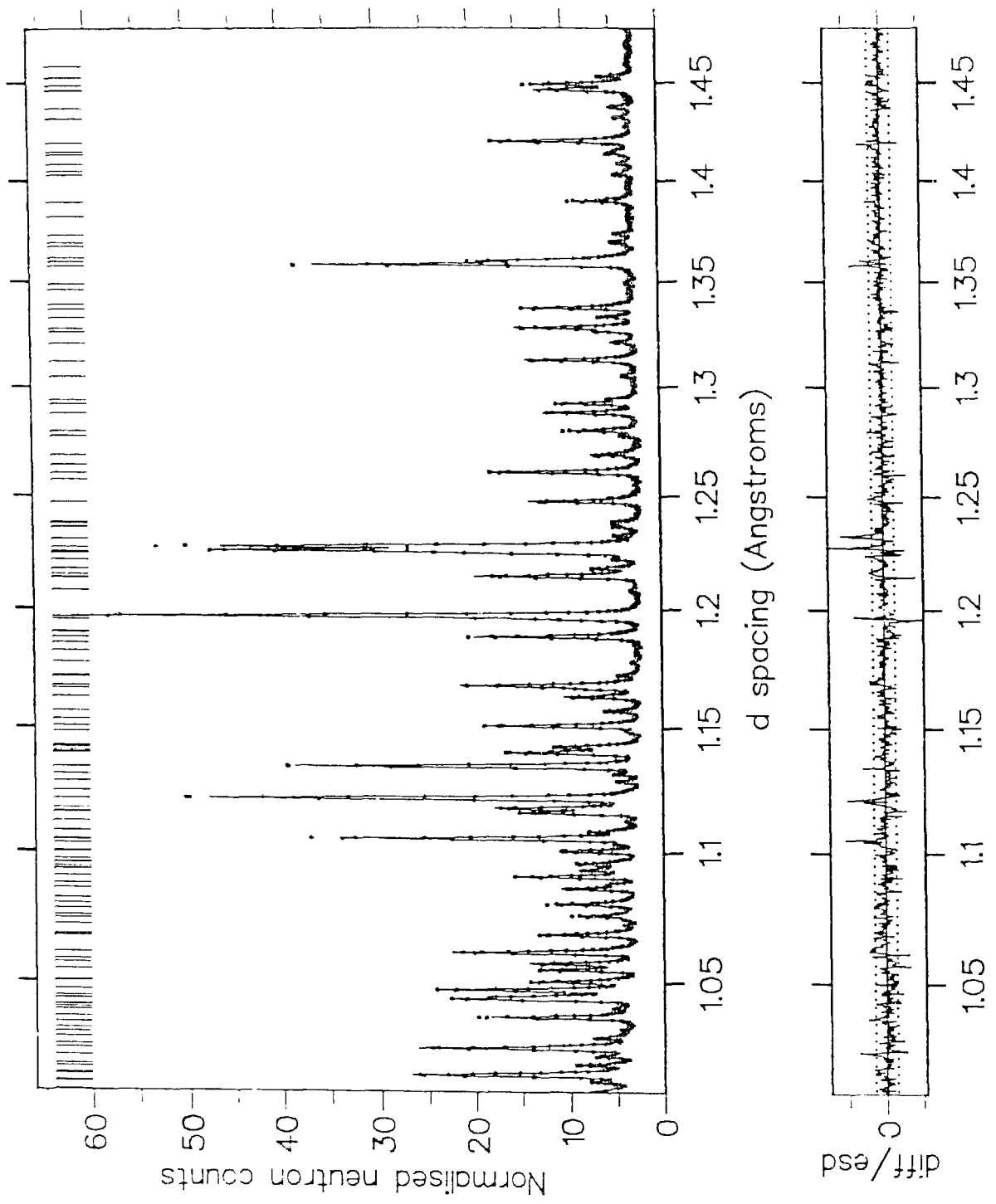
Normalised neutron counts
0
10
20
30
40
50
60
1.05
1.1
1.15
1.2
1.25
1.3
1.35
1.4
1.45
d spacing (Angstroms)
diff/esd
0
1.05
1.1
1.15
1.2
1.25
1.3
1.35
1.4
1.45

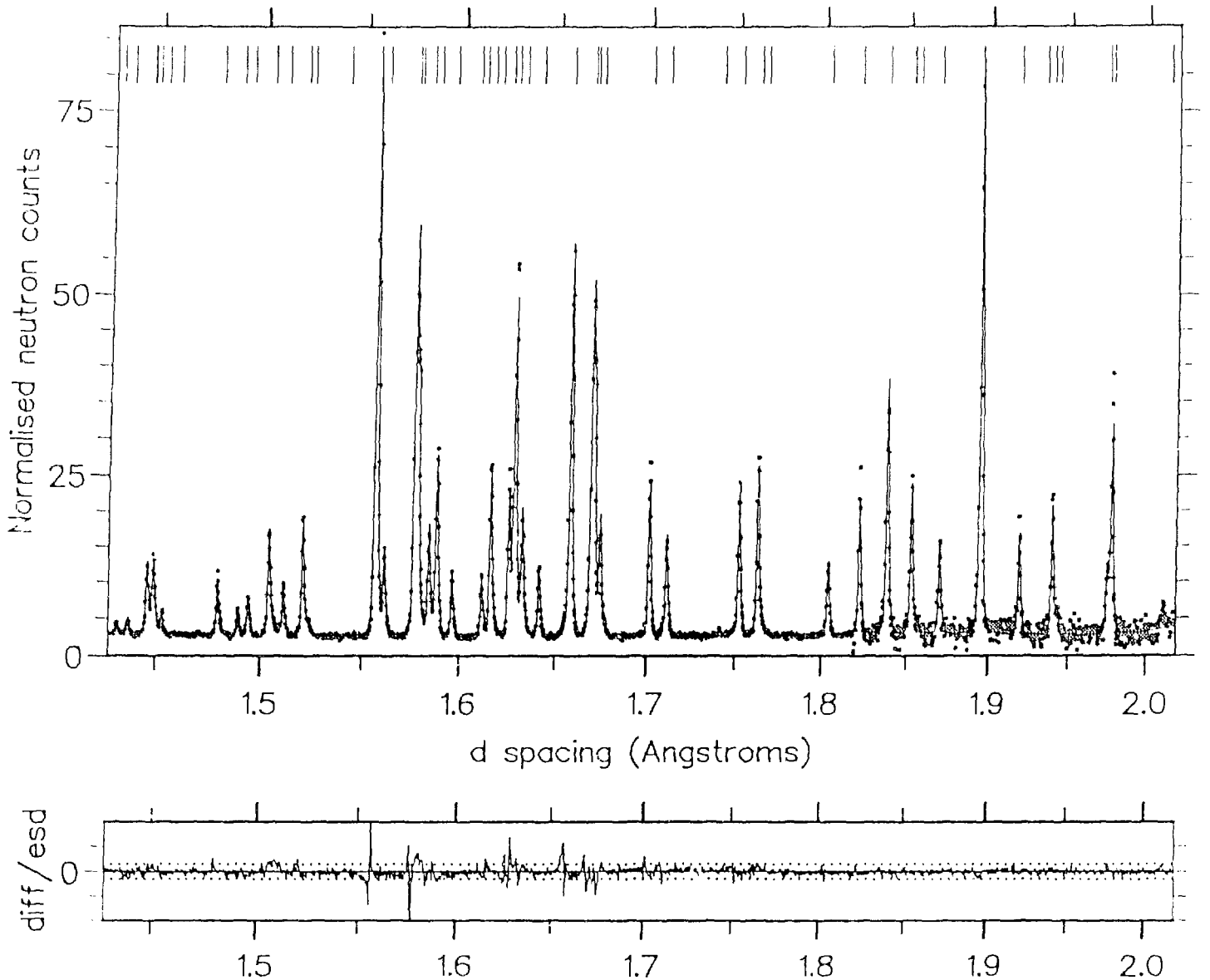
Normalised neutron counts
75
50
25
0
1.5
1.6
1.7
1.8
1.9
2.0
d spacing (Angstroms)
diff / esd
0
1.5
1.6
1.7
1.8
1.9
2.0

Fig 10(a)

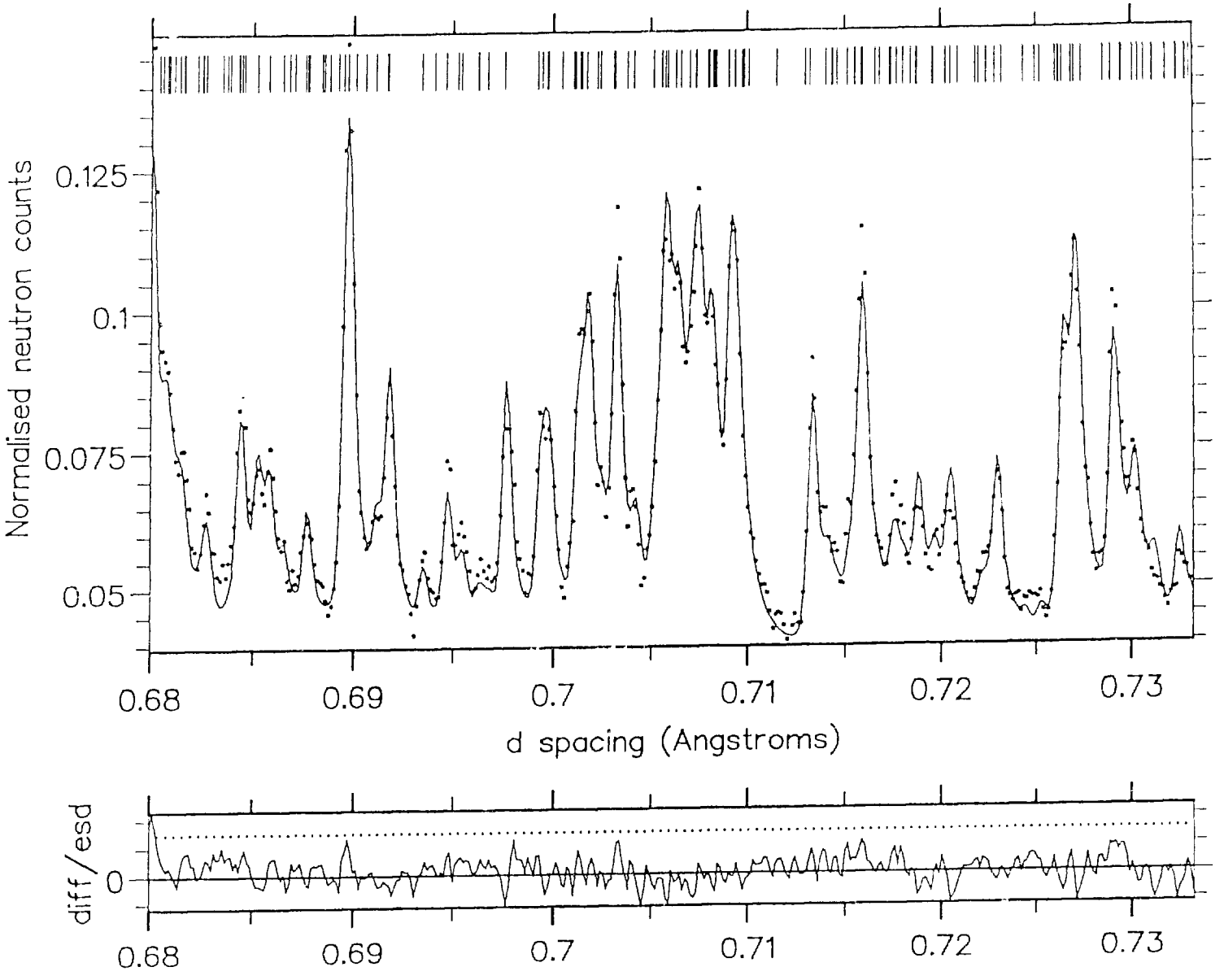
Normalised neutron counts
0.125
0.1
0.075
0.05
0.68
0.69
0.7
0.71
0.72
0.73
d spacing (Angstroms)
diff/esd
0
0.68
0.69
0.7
0.71
0.72
0.73

Fig 10(e)

Fig 10(f)

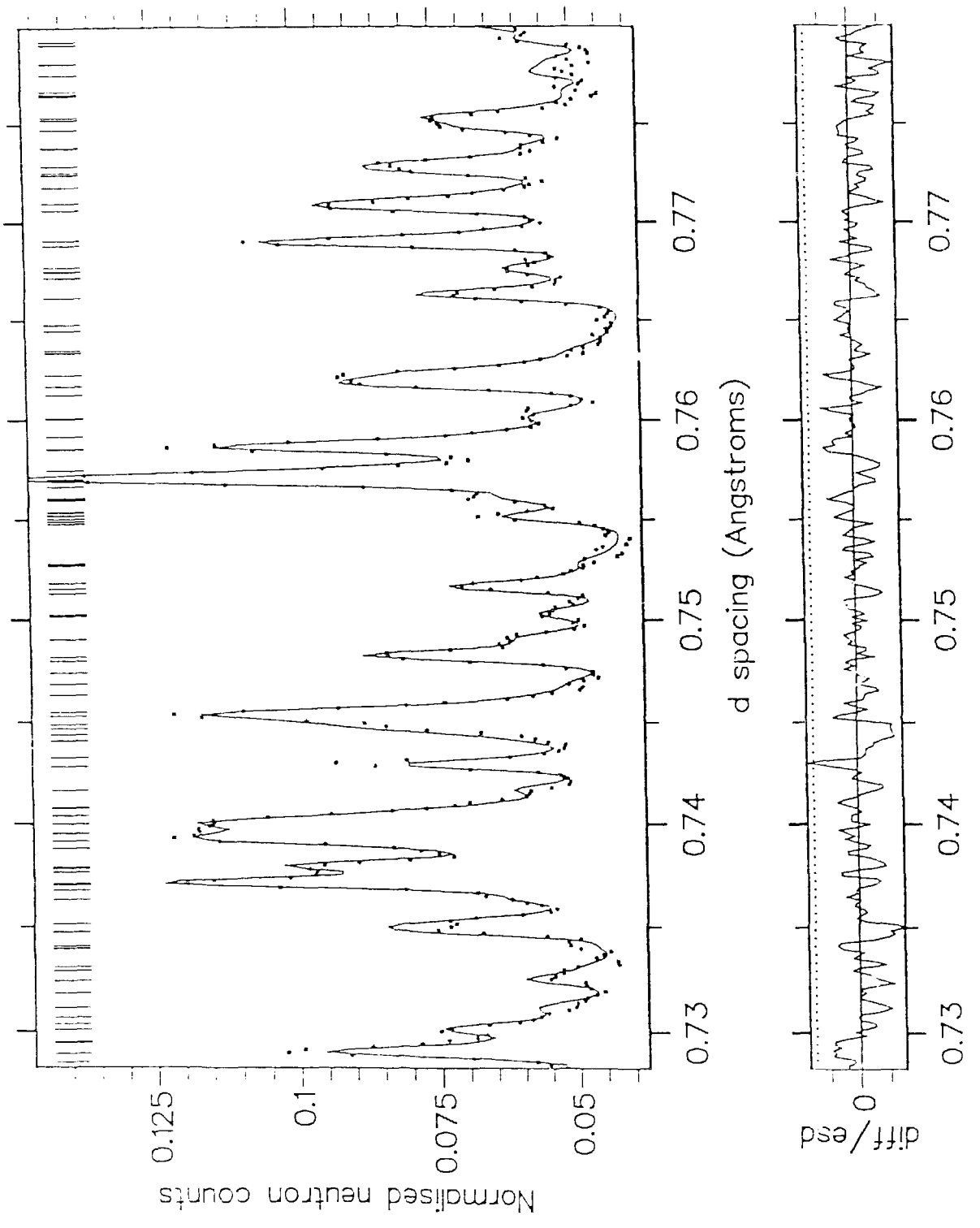
Normalised neutron counts
0.125
0.1
0.075
0.05
0.73
0.74
0.75
0.76
0.77
d spacing (Angstroms)
diff/esd
0
0.73
0.74
0.75
0.76
0.77

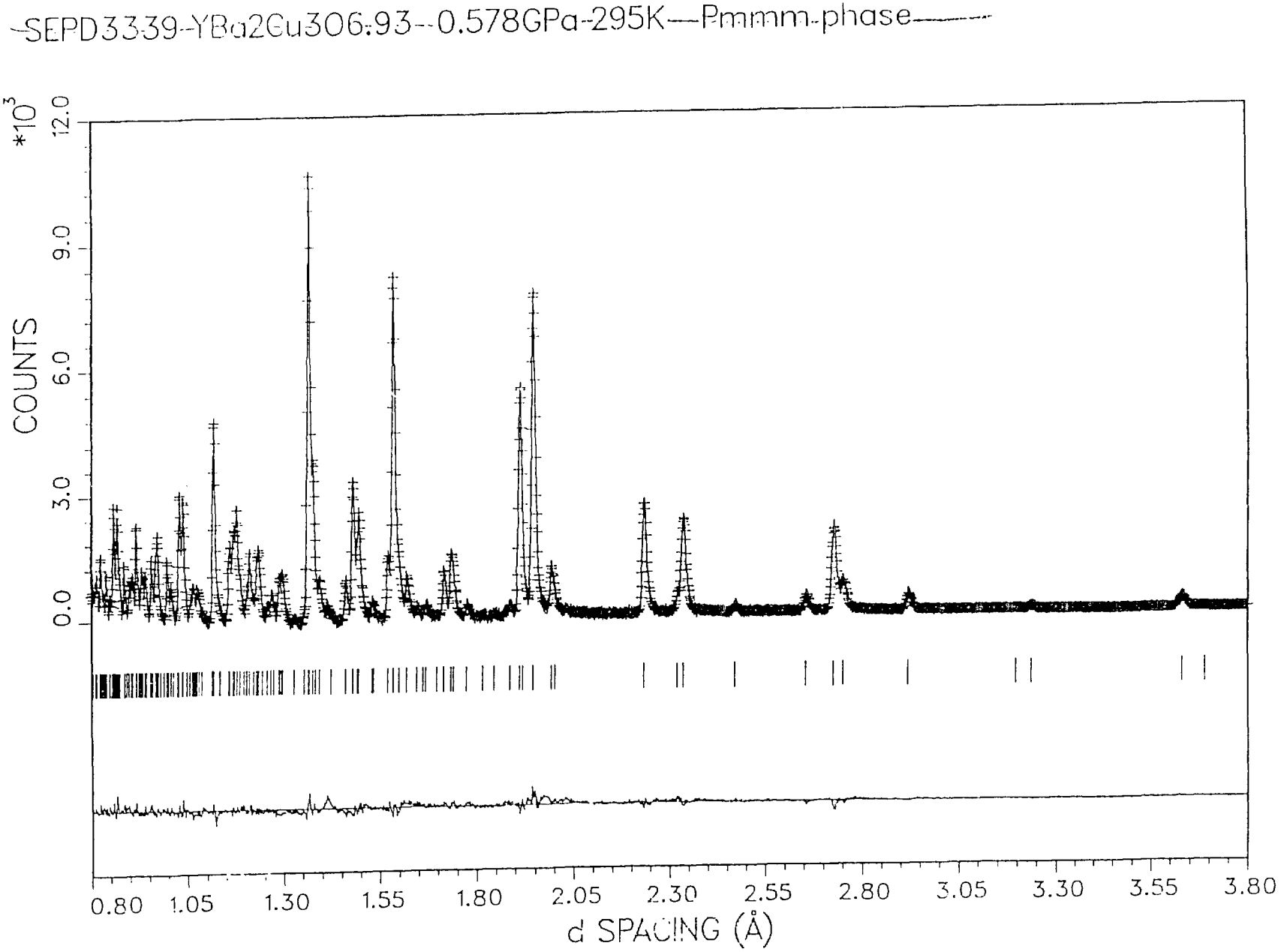
SEPD3339-YBa2Cu3O6.93--0.578GPa-295K---Pmmm-phase
*10^3
12.0
9.0
6.0
3.0
0.0
COUNTS
0.80
1.05
1.30
1.55
1.80
2.05
2.30
2.55
2.80
3.05
3.30
3.55
3.80
d SPACING (Å)

Fig 11

Fig #12

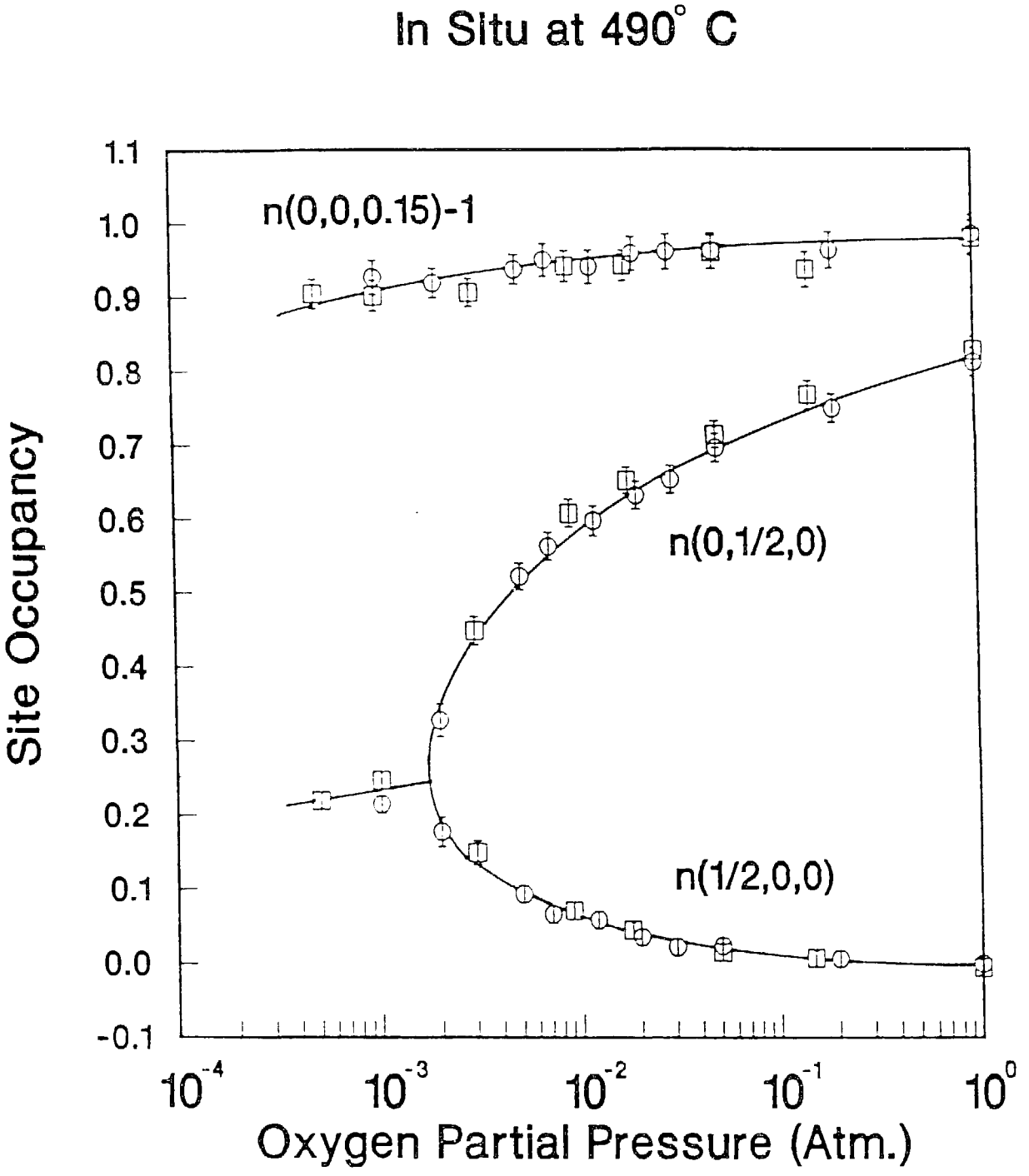
In Situ at 490° C
n(0,0,0.15)-1
n(0,1/2,0)
n(1/2,0,0)
Site Occupancy
1.1
1.0
0.9
0.8
0.7
0.6
0.5
0.4
0.3
0.2
0.1
0.0
-0.1
10^-4
10^-3
10^-2
10^-1
10^0
Oxygen Partial Pressure (Atm.)